TOWARD A UNIFICATION OF STAR FORMATION RATE DETERMINATIONS IN THE MILKY WAY AND OTHER GALAXIES

Laura Chomiuk[1,2] and Matthew S. Povich[3,4]

[1] National Radio Astronomy Observatory, P.O. Box O, Socorro, NM 87801, USA; lchomiuk@cfa.harvard.edu
[2] Harvard–Smithsonian Center for Astrophysics, MS-66, 60 Garden Street, Cambridge, MA 02138, USA
[3] Department of Astronomy and Astrophysics, The Pennsylvania State University, 525 Davey Lab,
University Park, PA 16802, USA; povich@astro.psu.edu

ABSTRACT

The star formation rate (SFR) of the Milky Way remains poorly known, with often-quoted values ranging from 1 to $10\,M_\odot\,\mathrm{yr}^{-1}$. This situation persists despite the potential for the Milky Way to serve as the ultimate SFR calibrator for external galaxies. We show that various estimates for the Galactic SFR are consistent with one another once they have been normalized to the same initial mass function (IMF) and massive star models, converging to $1.9 \pm 0.4\,M_\odot\,\mathrm{yr}^{-1}$. However, standard SFR diagnostics are vulnerable to systematics founded in the use of indirect observational tracers sensitive only to high-mass stars. We find that absolute SFRs measured using resolved low/intermediate-mass stellar populations in Galactic H II regions are systematically higher by factors of $\sim$2–3 compared with calibrations for SFRs measured from mid-IR and radio emission. We discuss some potential explanations for this discrepancy and conclude that it could be allayed if (1) the power-law slope of the IMF for intermediate-mass ($1.5\,M_\odot < m < 5\,M_\odot$) stars were steeper than the Salpeter slope or (2) a correction factor was applied to the extragalactic $24\,\mu\mathrm{m}$ SFR calibrations to account for the duration of star formation in individual mid-IR–bright H II regions relative to the lifetimes of O stars. Finally, we present some approaches for testing whether a Galactic SFR of $\sim 2\,M_\odot\,\mathrm{yr}^{-1}$ is consistent with what we would measure if we could view the Milky Way as external observers. Using luminous radio supernova remnants and X-ray point sources, we find that the Milky Way deviates from expectations at the 1σ–3σ level, hinting that perhaps the Galactic SFR is overestimated or extragalactic SFRs need to be revised upward.

Key words: galaxies: star formation – Galaxy: fundamental parameters – H II regions – ISM: supernova remnants

1. INTRODUCTION

Measuring the star formation rate (SFR) of a galaxy is like taking its pulse. The SFR quantifies the population of massive stars, which sets the composition and energetics of the interstellar medium (ISM) as well as the rate at which the ISM is dispersed through galactic winds and locked away into long-lived, low-mass stars. Our understanding of galaxy activity and the growth of stellar mass throughout cosmic time depends critically on measurements of SFR (e.g., Madau et al. 1996; Bouwens et al. 2011). Galaxy evolution models require the SFR as a fundamental input parameter (Larson 1974; Chiappini et al. 1997; Kauffmann & Haehnelt 2000; de Rossi et al. 2009), since the SFR sets both the level of massive star feedback and the rate at which gas and dust are depleted.

The Milky Way is generally excluded from comparative studies of star-forming galaxies because we lack a unified, global picture of its structure and star formation activity. The location of the solar system inside the Galactic disk gives us a disadvantaged perspective when attempting to study the Milky Way as a whole galaxy. Sightlines through the disk suffer very high extinction due to the dusty ISM, so SFR diagnostics which depend upon optical/UV observational tracers (e.g., Hα) cannot be applied to the Milky Way, just as they cannot be applied to external galaxies viewed nearly edge-on (see, e.g., Kennicutt 1998a and Calzetti et al. 2009 for reviews of SFR indicators). Radio and far-infrared (far-IR) observations are unaffected by extinction and therefore have provided most of the Galactic SFR estimates (e.g., Miller & Scalo 1979; Güsten & Mezger 1982; Misiriotis

et al. 2006; Murray & Rahman 2010). These wavelengths show great promise for providing convergence between extragalactic and Galactic SFR measurements, because a calibration like the Calzetti et al. (2007, hereafter C+07) $24\,\mu\mathrm{m}$ diagnostic for individual star-forming regions could be extended to the Galactic case. There remain, however, significant challenges stemming from uncertain distances to Galactic H II regions and confusion of multiple star formation regions overlapping along a given line of sight.

In spite of the observational challenges created by extinction, uncertain distances, and confusion, the Milky Way *should* be the ultimate SFR calibrator. The Galaxy offers the overwhelming advantage of high spatial resolution. Infrared observatories have advanced to the point that it is now routine to resolve individual stars in young embedded clusters several kiloparsecs distant. This makes it possible to directly probe the young stellar populations in massive clusters ionizing Galactic H II regions, constraining the stellar initial mass function (IMF) and stellar ages and investigating the detailed physical processes governing star formation. The resulting detailed star formation histories of Galactic H II regions and the associated molecular clouds can then be calibrated against diffuse emission tracers, like integrated IR luminosity, that are used to study star formation in external galaxies.

This paper seeks to answer three questions. (1) What are current estimates of the SFR of the Milky Way, and are they consistent with one another? Estimates have been presented in the literature for the past 35 years, ranging from $\sim 1\,M_\odot\,\mathrm{yr}^{-1}$ (Robitaille & Whitney 2010) to $\sim 10\,M_\odot\,\mathrm{yr}^{-1}$ (Güsten & Mezger 1982). Some of this variance is due to fundamental differences in the data, but, as we will demonstrate, systematics like the

use of different IMFs or stellar models play a significant role. (2) How solidly are *absolute* SFRs known? To relate SFRs to other physical quantities like gas masses and stellar masses, it is not enough to calibrate SFRs in a relative sense; we need to know that a measured SFR of $1\,M_\odot\,\mathrm{yr}^{-1}$ actually corresponds to $1\,M_\odot\,\mathrm{yr}^{-1}$ of material incorporated into stars. And finally, (3) Do Galactic SFR measurements give results consistent with extragalactic SFR diagnostics? Studies of the Galactic SFR generally use fundamentally different strategies compared with estimates of extragalactic SFRs; for example, Hα is not a useful diagnostic in the Galactic plane because of high extinction, and most external galaxies are too distant to study their resolved stellar populations. We would like to be certain that, if we measure $1\,M_\odot\,\mathrm{yr}^{-1}$ of star formation in an external galaxy, the same conditions in the Milky Way would also produce a measured SFR of $1\,M_\odot\,\mathrm{yr}^{-1}$. We identify two SFR diagnostics which can be applied in both the Milky Way and external galaxies: a galaxy's most luminous supernova remnant (SNR) and its population of X-ray point sources.

Note that throughout this work we use the standard term "Galactic SFR" to refer to the SFR of the Milky Way and "extragalactic SFRs" when referring to external galaxies. The subsequent sections of this paper are organized as follows: in Section 2, we define the IMF and stellar population synthesis models used as input assumptions in our SFR determinations, and in Section 3 we correct for these systematics in an effort to homogenize Galactic SFR estimates as much as possible. In Section 4, we derive the SFR in a sample of Galactic H II regions from their resolved stellar populations and discuss the results in the context of systematic errors inherent in absolute SFR determinations. In Section 5, we present SFR tracers that can be self-consistently applied both to the Milky Way and to external galaxies. We summarize our conclusions in Section 6.

2. OUR ASSUMED INPUTS FOR CALCULATING SFRs

As all SFR diagnostics only probe a subset of stellar masses, the IMF is a critical assumption in SFR estimates. The IMF is often expressed as $\phi(\log m) = dN/d\log m$, the number of stars in the logarithmic mass interval between $\log m$ and $\log m + d\log m$. We normalize our results to the commonly used "broken power-law" Kroupa IMF (Kroupa & Weidner 2003; used in the SFR calibrations of Kennicutt et al. 2009, hereafter K+09):

$$\phi(\log m) \propto m^{-\Gamma}, \qquad (1)$$

$$\Gamma = 0.3; \quad 0.1\,M_\odot < m < 0.5\,M_\odot, \qquad (2)$$

$$\Gamma = 1.3; \quad 0.5\,M_\odot < m < 100\,M_\odot. \qquad (3)$$

It is worth noting that the Chabrier (2005) IMF yields total stellar masses that are practically identical to the Kroupa IMF when both functions are normalized to high stellar masses (see Figure 1), implying that the SFRs calculated in this work should also represent SFRs assuming a Chabrier IMF.

Most SFR diagnostics indirectly measure a specific electromagnetic signature of massive stars, usually Lyman continuum (hydrogen-ionizing) photon flux, and then extrapolate this to a larger stellar population. Therefore, to accurately compare SFRs, we must use the same stellar population models and Lyman continuum photon rates in all cases. Here, we will use the stellar population models employed in version 5.1 of Starburst99[5] (Leitherer et al. 1999; Vázquez & Leitherer 2005)

---

[5] http://www.stsci.edu/science/starburst99/docs/

and used in the SFR calibration of K+09, assuming solar metallicity. These make use of the recent O star models of Smith et al. (2002) and Martins et al. (2005).

According to Kennicutt et al. (1994) and Kennicutt (1998a), an SFR of $1\,M_\odot\,\mathrm{yr}^{-1}$ produces a Lyman continuum photon rate $N_c = 9.26 \times 10^{52}$ photons s^{-1} for the Salpeter (1955) IMF (assuming a mass range of 0.1–100 $M_\odot$). The ratio of SFR to Lyman continuum photon rate is 1.44 times smaller for the Starburst99/Kroupa IMF formulation than for the Salpeter IMF (K+09), so we will adopt the following relationship between Lyman continuum rate and SFR for the Starburst99/Kroupa IMF calibration:

$$\mathrm{SFR}[M_\odot\,\mathrm{yr}^{-1}] = 7.5 \times 10^{-54} N_c[\mathrm{photons\,s}^{-1}]. \qquad (4)$$

This relationship will be used to compare Galactic SFR determinations throughout this paper.

Equation (4) should be interpreted as the continuous SFR required to maintain a steady-state population of ionizing stars that produces an observed ionizing photon rate N_c. The "steady state" condition requires that the ionizing-star birth rate balance the death rate. The timescale tacitly assumed by Equation (4) to compute SFRs is thus the lifetime of the ionizing stars. Simple experiments with the Starburst99 code, assuming a constant SFR, demonstrate that ongoing star formation must last a minimum time of ~8 Myr (the lifetime of a late O star) to reach the steady-state value of N_c, and N_c is within 5% of the steady-state value by ~5 Myr, the lifetime of an early O star (Bertelli et al. 1994; Martins et al. 2005). Unsurprisingly, O stars completely dominate the ionizing photon flux from actively star-forming populations. We caution that the steady-state approximation *underestimates* SFRs for stellar populations with durations of star formation significantly less than O-star lifetimes. We will bear this issue in mind throughout Section 3.1 and return to it in Section 4.3.7 below.

Where we determine SFRs from SN rates instead of Lyman continuum photon rates, we assume Padova isochrones (Bertelli et al. 1994) and that stars in the mass range from 10 to $100\,M_\odot$ explode as SNe. To determine SFRs in individual star-forming regions from intermediate-mass star counts, we also assume a Kroupa IMF and use stellar population ages from the literature, which generally are based on pre-main-sequence (PMS) isochrones (Siess et al. 2000).

3. REVIEW OF MILKY WAY STAR FORMATION RATE ESTIMATES

3.1. Lyman Continuum Photon Rates

Smith et al. (1978) established the "canonical" value for the Galactic SFR by calculating the total Lyman continuum photon rate required to maintain the ionization of all Galactic giant H II regions then known from radio continuum surveys. They reported $N_c = 4.7 \times 10^{52}$ photons s^{-1} (shown by later studies to be a lower limit) based on the thermal free–free radio continuum flux emitted by the Galactic H II regions in their sample, using the formulation in Mezger et al. (1974) and correcting for a factor of ~2 internal absorption of Lyman continuum photons by dust. Smith et al. (1978) then used a Salpeter (1955) IMF (with limits of 0.1 and 100 $M_\odot$), the massive star models of Panagia (1973), and an (unrealistically low) assumed average duration of star formation in a Galactic radio H II region of 5×10^5 yr to transform from Lyman continuum photon rate to a Galactic SFR of ~5 $M_\odot\,\mathrm{yr}^{-1}$ (factor
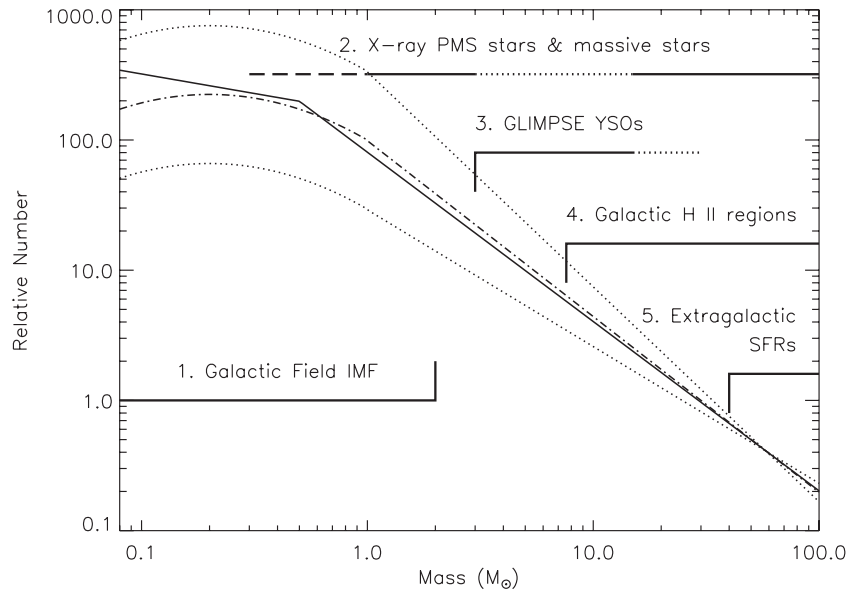
Figure 1. Simulated Galactic-field IMF (solid curve; Kroupa & Weidner 2003) and lognormal + power-law IMF (dash-dotted curve; Chabrier 2005) normalized to the same relative numbers of early O-type stars ($m > 40\,M_\odot$). Dotted curves show an error envelope on the Chabrier IMF based on an uncertainty of 0.3 in the value of the power-law slope for $m > 1\,M_\odot$. Five mass ranges (numbered) relevant to multi-wavelength determinations of the IMF and SFRs are indicated schematically by brackets and discussed in the text.

Table 1
Normalized SFR Estimates for the Milky Way

Method	Observation	SFR ($M_\odot$ yr^{-1})	Reference
Ionization rate	Radio Free–Free	0.35	Smith et al. (1978)
Ionization rate	Radio Free–Free	2.0 ± 0.6	Güsten & Mezger (1982)
Ionization rate	Radio Free–Free	1.6 ± 0.5	Mezger (1987)
Ionization rate	*COBE* N II 205 μm	2.6 ± 1.3	Bennett et al. (1994)
Ionization rate	*COBE* N II 205 μm	2.0 ± 1.0	McKee & Williams (1997)
SN rate	O/B Star Counts	1.8 ± 0.6	Reed (2005)
Nucleosynthesis	INTEGRAL Gamma-ray ^{26}Al	2.0 ± 1.2	Diehl et al. (2006)
Dust heating	*COBE* FIR continuum	1.9 ± 0.8[a]	Misiriotis et al. (2006)
Ionization rate	*WMAP* Free–Free	2.4 ± 1.2[a]	Murray & Rahman (2010)
YSO star counts	*Spitzer* IR Photometry	1.1 ± 0.4	Robitaille & Whitney (2010)
YSO star counts	*MSX* IR Photometry	1.8 ± 0.3	Davies et al. (2011)

Note. [a] Assumed 50% uncertainty, as no error is quoted by the original author.

of ~3 reported uncertainty). Their measurement of N_c translates to a Galactic SFR of 0.35 $M_\odot$ yr^{-1} with the Starburst99/Kroupa IMF calibration used here (Table 1). This strikingly low value can largely be explained by the incompleteness of their H II region sample, but is also contributed to by the inappropriateness of the Starburst99 steady-state calibration (Equation (4)) as applied to the young H II regions in the Smith et al. sample (this will be discussed further in Section 4.3).

Building upon the work of Smith et al. (1978), Güsten & Mezger (1982) made a new estimate of the Galactic SFR from radio H II regions, taking into account the thermal radio emission from "extended low-density" H II regions and including Lyman continuum photons escaping from giant H II regions. They measured $N_c = (2.7 \pm 0.8) \times 10^{53}$ photons s^{-1}, nearly six times the Smith et al. value, and reported a Galactic SFR of 11 $M_\odot$ yr^{-1}, which is clearly *not* six times the SFR estimate of 5 $M_\odot$ yr^{-1} made by Smith et al. (1978). This discrepancy is explained by the adoption of the lognormal IMF of Miller & Scalo (1979), different limits on the IMF mass range (from 0.1 to 60 $M_\odot$), and different stellar models (see Appendix A

of Güsten & Mezger 1982 for a description of their conversion from Lyman continuum photon rate to stellar mass). In our homogenized Starburst99/Kroupa IMF calibration, the Güsten & Mezger (1982) measurement of N_c translates to an SFR of $2.0 \pm 0.6\,M_\odot$ yr^{-1} (Table 1). The incorporation of low-density H II regions means that this measurement included the contribution to ionization provided by older Galactic O stars omitted by Smith et al. (1978); hence the steady-state calibration should be appropriate here.

Mezger (1987) calculated a slightly lower value for the Lyman continuum photon rate of $N_c = (2.1 \pm 0.6) \times 10^{53}$ photons s^{-1}, discrepant from their earlier value due to their use of $R_\odot = 8.5$ kpc for the distance to the Galactic center (as opposed to $R_\odot = 10$ kpc used by Güsten & Mezger 1982). This discrepancy underscores the point that Galactic SFR measurements are often dependent on models of Milky Way structure and star formation therein. Here, we are not accounting for differences in the assumed Milky Way model. They also used a modified Miller–Scalo IMF with a less steep slope for the highest mass stars, and find an SFR of $5.7 \pm 1.6\,M_\odot$ yr^{-1}. Using our

3

Starburst99/Kroupa IMF calibration, we find a corresponding SFR of $1.6 \pm 0.5 \, M_\odot \, \mathrm{yr}^{-1}$.

Bennett et al. (1994) used *Cosmic Background Explorer* (*COBE*) observations of N II 205 μm emission to measure the rate of Lyman continuum photons in the Milky Way, and, correcting for dust absorption and photon escape, they found $N_c = (3.5 \pm 1.8) \times 10^{53}$ photons s^{-1}. Subsequently, McKee & Williams (1997) used the same *COBE* data and slightly different assumptions to measure a Lyman continuum photon rate of $N_c = (2.6 \pm 1.3) \times 10^{53}$ photons s^{-1}. These two estimates of N_c agree with one another to within the 50% uncertainties quoted by the authors and are also in excellent agreement with the radio data from Güsten & Mezger (1982).

In a recent update to the original Galactic SFR estimates, Murray & Rahman (2010) used *Wilkinson Microwave Anisotropy Probe* (*WMAP*) observations of free–free emission to measure a dust-corrected Lyman continuum photon rate of $N_c = 3.2 \times 10^{53}$ photons s^{-1}. This is in good agreement with previous measurements of N_c and corresponds to an SFR of $2.4 \, M_\odot \, \mathrm{yr}^{-1}$ (Table 1). The *COBE* and *WMAP* studies utilize the integrated light of the Milky Way and average over its entire stellar population; therefore, the steady-state Starburst99 calibration is also appropriate to these studies.

3.2. Massive Star Counts and Supernova Rates

Measurements of the core-collapse SN rate in the Milky Way have also been used to constrain the SFR. An SN rate of 0.85 events per century is expected for an SFR of $1 \, M_\odot \, \mathrm{yr}^{-1}$, assuming a Kroupa IMF and an SN progenitor mass range of 10–100 $M_\odot$ (calculated using Starburst99 models with the parameters discussed in Section 2).

Reed (2005) surveyed the B2–O3 type stars ($\geqslant 10 \, M_\odot$) in the local solar neighborhood (within 1.5 kpc) and assumed a model of the Milky Way to extrapolate these massive star counts to the entire Galaxy. He estimated a steady-state SN rate of one to two events per century, averaged over the lifetimes of massive stars (~ 20 Myr for 10 $M_\odot$). In our Starburst99/Kroupa IMF calibration, this translates to an SFR of 1.2–$2.4 \, M_\odot \, \mathrm{yr}^{-1}$.

Diehl et al. (2006) used gamma-ray measurements of radioactive ^{26}Al to constrain the core-collapse SN rate in the Milky Way to 1.9 ± 1.1 events century^{-1}, averaged over a timescale set by the half life of ^{26}Al ($\sim 7.2 \times 10^5$ yr). They assumed a Scalo (1998) IMF with $\Gamma = 1.7$ and an SN progenitor mass range of 10–120 $M_\odot$. Assuming massive star yields of ^{26}Al as modeled by Limongi & Chieffi (2006), the yields for a Kroupa IMF are a factor of 1.12 higher than for the Scalo IMF. This means that for our normalized assumptions, the SN rate from radioactive ^{26}Al is 1.7 ± 1.0 events century^{-1}, consistent with the results from Reed (2005). This translates to an SFR of $2 \pm 1.2 \, M_\odot \, \mathrm{yr}^{-1}$.

3.3. Infrared Diffuse Emission and Point Sources

Misiriotis et al. (2006) constructed a model of the spatial distribution of stars, gas, and dust in the Galaxy constrained by *COBE* observations of the Galactic IR emission. They measured the 100 μm luminosity of the Milky Way and, using the conversion described in Misiriotis et al. (2004), calculated an SFR of $2.7 \, M_\odot \, \mathrm{yr}^{-1}$. However, they used a Salpeter IMF (0.1–100 $M_\odot$) and Fioc & Rocca-Volmerange (1997) stellar population models. We attempt to correct for the difference in IMF by dividing the SFR by 1.44 (as above, see Equation (4)), assuming that the Lyman continuum photons and the non-ionizing UV photons which produce FIR emission scale together

(a good assumption, as the disparity between the Salpeter and Kroupa IMFs occurs at low stellar masses). Typically, galaxy-wide mid-IR measurements of SFR are sensitive to star formation over longer timescales than other SFR diagnostics (~ 100 Myr; C+07), as even non-ionizing B stars can contribute significantly to dust heating (Cox et al. 1986). We note that FIR diagnostics of the SFR include a host of critical assumptions, like what fraction of stellar light is absorbed by dust and how much older stellar populations contribute to dust heating. Still, the estimate of Galactic SFR from Misiriotis et al. (2006) is consistent with the others described here, at $1.9 \, M_\odot \, \mathrm{yr}^{-1}$ (Table 1).

Robitaille & Whitney (2010) produced Galactic population synthesis models of young stellar objects (YSOs) that still retain dusty circumstellar disks and/or natal envelopes, assuming a Kroupa IMF, a simple prescription for accretion, and a YSO lifetime of 2 Myr. These population synthesis models were then used to simulate the Robitaille et al. (2008) catalog of YSOs identified via mid-IR excess emission from the *Spitzer Space Telescope* GLIMPSE (Galactic Legacy Infrared Mid-Plane Survey Extraordinaire; Churchwell et al. 2009) surveys of the Galactic plane. By comparing the simulations to the catalog, Robitaille & Whitney (2010) derived an SFR of 0.68–1.45 $M_\odot \, \mathrm{yr}^{-1}$. Robitaille & Whitney (2010) note that their quoted range of SFRs includes only the uncertainties on the total number of YSOs in the Robitaille et al. (2008) catalog.

Davies et al. (2011) modeled massive ($m > 8 \, M_\odot$) YSOs found in the Red *MSX* Sources (RMSs) Survey, using the data to find the best fits to basic YSO parameters such as bolometric luminosity and mass. This study assumed a massive YSO lifetime of ~ 0.1 Myr and a Kroupa IMF, resulting in a Galactic SFR of 1.5–2.0 $M_\odot \, \mathrm{yr}^{-1}$.

3.4. Galactic SFR Determinations Compared

We see remarkably good agreement in Table 1 between estimates of the Galactic SFR (with the exception of the oldest, Smith et al. 1978, which was clearly incomplete and superseded by Güsten & Mezger 1982), after we have taken care to normalize assumptions about the parent stellar populations. The estimates cluster around an average of $1.9 \pm 0.4 \, M_\odot \, \mathrm{yr}^{-1}$ (excluding Smith et al. 1978 and Güsten & Mezger 1982, which were both improved upon by Mezger 1987). The most significant outlier is the result from Robitaille & Whitney (2010). We note that their Galactic SFR could be regarded as a lower limit, due both to issues of completeness and to the 2 Myr lifetime of the YSO phase used in their preliminary population synthesis models. This age limit is likely an overestimate because it is based on circumstellar disk lifetimes for low-mass PMS stars, while the Robitaille et al. (2008) catalog is sensitive primarily to intermediate-mass YSOs (masses $> 3 \, M_\odot$). There is mounting evidence that the optically thick inner disks of intermediate-mass YSOs are rapidly destroyed over timescales < 1 Myr (Povich & Whitney 2010; Koenig & Allen 2011; Povich et al. 2011). Such a correction in a future update of the Robitaille & Whitney (2010) population synthesis models could easily provide the factor of ~ 2 increase necessary to bring the Galactic SFR from intermediate-mass YSO star counts into agreement with the other estimates.

We stress that our homogenized estimate is significantly different from the Galactic SFR of 4–5 $M_\odot \, \mathrm{yr}^{-1}$ often quoted in the literature, and this disparity is due only to differences in the IMF and stellar models used. Investigators hoping to compare properties of the Milky Way with other galaxies (e.g., the

luminosity functions (LFs) of star clusters; Hanson & Popescu 2008) must first calibrate the SFRs to the same scale. The Starburst99/Kroupa IMF calibration is likely to be used often in the future, in which case the corresponding Galactic SFR is $2\,M_\odot\,\mathrm{yr}^{-1}$.

4. CALIBRATING SFR DIAGNOSTICS AGAINST DIRECT STAR COUNTS

We have demonstrated that various measurements of the Galactic SFR using myriad observational tracers converge to a consistent value, provided that systematic differences are minimized by adopting a uniform IMF and stellar models. We have made no assertions that our assumed inputs for calculating SFRs (Section 2) are the correct ones; they were chosen simply to match the Starburst99 stellar population synthesis models widely applied to SFR determinations in external galaxies. If these assumptions were incorrect, then *relative* SFR comparisons would be unaffected, but potentially large systematic errors would be introduced into *absolute* SFR determinations.

While the general broken-power-law (or lognormal + power-law; Chabrier 2003) form of the observed IMF is remarkably consistent across stellar populations in widely disparate environments, variations have been reported both in the power-law slopes and in the locations of the break points where the slopes change (Kroupa 2001; Bastian et al. 2010). Although these variations have low significance given the typically large uncertainties inherent in IMF measurements (Bastian et al. 2010), even an insignificant deviation from the default Salpeter–Kroupa slope can have significant consequences. The center of mass of the IMF, defined as the point where the integrated stellar mass is divided equally between higher and lower masses, falls near $1\,M_\odot$ (Kroupa 2001). If we estimate SFRs by extrapolating over an IMF that is pinned only to massive stars, we maximize the impact of IMF variations because such massive stars are farthest from the center of mass. This effect is illustrated in Figure 1, in which the lognormal + power-law ($\Gamma = 1.35$) IMF of Chabrier (2005) is plotted alongside the standard Kroupa IMF. Both IMF models have been normalized to the same relative numbers of very high-mass stars (early O stars with $m > 40\,M_\odot$, which dominate the bolometric luminosity and Lyman continuum photon flux in observable extragalactic star-forming regions; Martins et al. 2005). With this normalization, the Chabrier IMF yields 15% fewer stars (defined henceforth as $N_{\rm pop}$) but 3% greater integrated stellar mass ($M_{\rm pop}$) above the hydrogen-burning limit ($m \geqslant 0.08\,M_\odot$) compared to the Kroupa IMF. The insignificant difference in $M_{\rm pop}$ means that the choice between these IMFs is unimportant for deriving SFRs from unresolved stellar populations in H II regions. However, an uncertainty of 0.3 on the value of Γ (e.g., Muench et al. 2002; Chabrier 2005) increases $N_{\rm pop}$ by a factor of 2.3 and $M_{\rm pop}$ by a factor of 1.6 on the high side envelope (upper dotted curve in Figure 1).

High-resolution, wide-field, multi-wavelength imaging observations enable us to derive SFRs in bright Galactic H II regions (the nearby analogs of observable extragalactic star-forming regions) using *direct* detections of the resolved low- and intermediate-mass stellar populations. Such an approach samples the center of the IMF, greatly reducing the uncertainty of extrapolation (Figure 1) while avoiding altogether any dependence on models of massive star properties. Hence, the following analysis provides an independent estimate of the systematic errors on absolute SFR calibrations.

4.1. The Galactic H II Region M17 as a Case Study

4.1.1. The X-Ray Luminosity Function: SFR from Star Counts

We begin by considering the well studied, nearby (2.0 kpc; Xu et al. 2011) Galactic H II region M17. Because of its relatively high obscuration ($A_V > 8$ mag), bright nebulosity, and overwhelming field-star contamination produced by its location in the inner Galactic plane ($[l, b] = [15°.1, −0°.7]$), establishing a reliable membership catalog for NGC 6618, the massive cluster ionizing M17, has proven prohibitively difficult using optical/IR photometry alone (see discussions in Broos et al. 2007 and Povich et al. 2009). These problems have been overcome by employing high-resolution imaging spectroscopy from the Advanced CCD Imaging Spectrometer (ACIS) of the *Chandra X-ray Observatory* to identify cluster members (Broos et al. 2007). Low- and intermediate-mass PMS stars exhibit powerful convectively driven magnetic reconnection flaring activity; hence, they are 10^2–10^3 times more luminous in X-rays than older Galactic field stars, and their X-ray luminosity L_X is broadly correlated with bolometric luminosity and hence stellar mass (Preibisch & Feigelson 2005). Hard (>2 keV) X-ray photons are relatively unaffected by interstellar absorption, and while optical/IR photometry in bright H II regions is plagued by diffuse nebular emission, ACIS point-source detections generally do not suffer significant reductions in sensitivity due to diffuse emission (Broos et al. 2007).

The stellar X-ray luminosity function (XLF; the distribution of stars as a function of L_X) itself provides a good statistical tracer of the underlying IMF in young clusters (Getman et al. 2006; Wang et al. 2007). The approximate range of masses sampled by observed XLFs of various massive clusters is indicated in Figure 1. In addition to PMS stars, X-ray observations are highly sensitive to massive stars, which produce strong X-ray emission via microshocks in their stellar winds and a variety of more exotic mechanisms (Gagné et al. 2011). Intermediate-mass A- and B-type stars on or near the zero-age main sequence lack both magnetic dynamos and powerful stellar winds, and hence they are generally X-ray quiet (Povich et al. 2011 and references therein).

To estimate $N_{\rm pop}$ from the XLF of a given cluster, the simplest approach (e.g., Feigelson et al. 2011) is to use the XLF as a calibrator of the ONC, which contains 839 lightly obscured (X-ray median energy <2 keV), low-mass members (Getman et al. 2005). The XLF in the target cluster is compared to the calibrator ONC XLF to derive a scale factor, which is then multiplied by $N_{\rm pop}$(ONC), the population of the ONC above the brown-dwarf limit (Hillenbrand & Hartmann 1998).

Estimates of $N_{\rm pop}$ from XLF scaling assume several fundamental similarities between the target cluster and the ONC: (1) the form of the underlying IMF, (2) the ratio of obscured/unobscured cluster members, (3) the circumstellar disk fraction of the cluster membership (L_X is lower for protostars and YSOs with disks compared to diskless PMS stars of the same mass; see Povich et al. 2011 and references therein), and (4) the transformation between XLF and IMF. With the possible exception of (1), none of these assumptions is generally valid. Assumptions (3) and (4) could hold if the age of the target cluster is sufficiently close to that of the ONC, but in practice ages are difficult to determine, and in any case it is not yet known how much the target cluster could differ from the ONC age before producing a significant impact on the XLF scaling. To avoid assumption (2), a "two-component" approach can be employed, in which the cluster XLF is divided into lightly

obscured and heavily obscured sub-populations, and the calibrator ONC XLF is scaled independently to the XLF of each sub-population (this second approach was used by Broos et al. 2007).

In M17, the XLF was measured from 886 sources detected by *Chandra*/ACIS (Broos et al. 2007). Povich et al. (2009) showed that N_{pop} as reported by Broos et al. (2007) for NGC 6618 translates to an SFR based on star counts of $SFR_{SC} = 0.008$–$0.01\,M_\odot$ yr^{-1}, using the Muench et al. (2002) IMF to convert N_{pop} to M_{pop}. Adopting instead our standard Kroupa IMF and an upper envelope of 1.5 Myr (see discussion in Povich et al. 2009) for the age spread of the X-ray-detected stellar population in NGC 6618, SFR_{SC} becomes 0.004–0.006 $M_\odot$ yr^{-1}.

In the following two subsections, we estimate the M17 SFR using independent tracers of the massive stellar population and compare the results to $SFR_{SC} \sim 0.005\,M_\odot$ yr^{-1}.

4.1.2. The Thermal Radio Continuum SFR Diagnostic in M17

Historically there has been some disagreement between different measurements of the M17 radio continuum flux density. Adopting $S_{5\,GHz} = 784$ Jy and $S_{15\,GHz} = 609$ Jy from Povich et al. (2007) and using the same conversion from thermal continuum (free–free emission) to Lyman continuum photon rate as Smith et al. (1978), we calculate $N'_c = 3.07 \times 10^{50}$ s^{-1} at 5 GHz and 2.66×10^{50} s^{-1} at 15 GHz. The difference reflects a $\sim$15% uncertainty on N'_c.

Summing over the known O stars in NGC 6618 and using the models of Martins et al. (2005) to obtain the Lyman continuum photon emission rates as a function of spectral type, the combined Lyman continuum photon rate emitted is $N_c = 3 \times 10^{50}$ s^{-1}. This is in surprisingly good agreement with N'_c derived above, given that some fraction of the Lyman continuum photons are expected to be absorbed by dust before contributing to the ionization of the H II region, and some fraction of the Lyman continuum flux likely escapes from the nebula altogether (Povich et al. 2007). Our calculation of N_c largely neglected the contribution of stars later than O8 to the ionization, but the inclusion of O8–B3 stars would only increase N_c by a few percent. There may yet be new major ionizing stars waiting to be discovered in M17 (Povich et al. 2008 reported the discovery of a new candidate O5 V star), but it is unlikely that a significant fraction of the ionizing stellar population in M17 has been missed. We have accounted for known massive binaries among the majority of the principal ionizing stars (types O6 and earlier) in our calculation of N_c (Povich et al. 2009). We note that the total bolometric luminosity of the known O stars is $L_{OB} \sim 5.8 \times 10^6\,L_\odot$, in very good agreement with the luminosity in the global spectral energy distribution (SED) of the M17 nebula (Povich et al. 2007).

Absorption of Lyman continuum photons by dust has a negligible impact upon the ionization of M17. Somewhat more important is the escape of Lyman continuum photons into the diffuse ISM through the blow-out in the H II region (Povich et al. 2007). In the most probable nebular geometries, $N'_c/N_c \gtrsim 0.9$ (Povich et al. 2007). Given the uncertainty in N'_c, it is not unreasonable to assume $N_c = N'_c = 3 \times 10^{50}$ s^{-1} for this highly embedded H II region. Using our normalized conversion in Equation (4), this translates to $SFR_{ff} = 0.0022\,M_\odot$ yr^{-1} traced by free–free emission, which is *lower* than SFR_{SC} by a factor of $\gtrsim 2$. In Section 4.3, we will discuss some possible explanations for this discrepancy.

4.1.3. The 24 μm Mid-IR SFR Diagnostic in M17

According to C+07, their *Spitzer* 24 μm SFR calibration "is appropriate for metal-rich H II regions or starbursts" where the radiation field is dominated by young massive stars. M17 is a highly embedded Galactic H II region that radiates $\gtrsim$90% of its luminosity in the mid-IR (Povich et al. 2007), and hence it meets these criteria. We can therefore use M17 to test the applicability of the C+07 extragalactic mid-IR SFR diagnostic to a nearby, resolved H II region.

M17 was observed using the Multiband Imaging Photometer (MIPS) on board *Spitzer* as part of the MIPSGAL survey (Carey et al. 2009), but because the H II region is bright enough to completely saturate even the short MIPSGAL exposures at 24 μm, there is no direct measurement of the luminosity in the MIPS 24 μm band, L_{24}, that can be used as an input to the C+07 SFR relation (their Equation (9)). Instead, we interpolate the global SED presented by Povich et al. (2007) over the range of 20–60 μm and compute the 24 μm flux density, $F_\nu(24)$ (see Figure 2(a)). This gives

$$L_{24} \equiv \nu L_\nu(24) = 4\pi d^2 \nu F_\nu(24) = 6.6 \times 10^{39}\ \mathrm{erg\ s^{-1}} \quad (5)$$

($<$25% uncertainty, dominated by the uncertain distance d) and, following C+07, $SFR_{24} = SFR_{ff} = 0.0022\,M_\odot$ yr^{-1}, just as we derived from radio free–free emission above. We therefore find that SFRs based on independent indirect tracers of Lyman continuum photon rate are in agreement, but both are lower than SFR_{SC} by factors of $\gtrsim 2$. We note that the C+07 calibration uses the Kroupa IMF and Starburst99 models as we have used throughout this paper, including in our calculation of SFR_{ff}. As cautioned in Section 2, M17 may be too young for the steady-state approximation to hold. We will discuss the consequences of ignoring this caveat in Section 4.3.7.

The C+07 L_{24} SFR diagnostic is a statistical relation based on 179 observed H II region "knots" in 23 different high-metallicity galaxies, and its disagreement with SFR_{SC} in a single, Galactic H II region is hardly a cause for alarm. Perhaps M17 is simply an outlier from the trend, or perhaps there is some fundamental difference in measurement between the Galactic and extragalactic observations. Povich et al. (2007) measured the mid-IR luminosity of M17 using a large aperture chosen to match the linear extent of the H II region and photodissociation region, while the H II knots in distant galaxies were generally smaller than the apertures used by C+07 to extract their fluxes. Hence, there could be an offset between the mid-IR luminosity measured for M17 and the luminosities of the extragalactic H II knots due to the drastically different filling factors and background subtractions involved. The impact of such potential biases can be evaluated by hypothetically locating M17 among the C+07 extragalactic sample (their Figure 9). For each H II knot in their sample, C+07 measured "luminosity surface densities" (LSDs; units of erg s^{-1} kpc^{-2}) $S_{P\alpha}$ and S_{24} in the Pα recombination line and the MIPS 24 μm band, respectively, using a fixed photometric aperture matched to the MIPS 24 μm resolution. The aperture size corresponded to a linear scale of $\sim$300 pc at $d = 5$ Mpc.

Among the high-metallicity H II knots, the range of LSDs observed by C+07 was $38 \lesssim \log S_{P\alpha,corr} \lesssim 40$ and $40.5 \lesssim \log S_{24} \lesssim 42.5$. An H II region with the same L_{24} as M17, located in a galaxy 5 Mpc distant, would have an observed LSD of $\log S_{24} = 41.00$, well within the range. We can calculate the luminosity $L_{P\alpha}$ in the Pα line from the thermal radio continuum
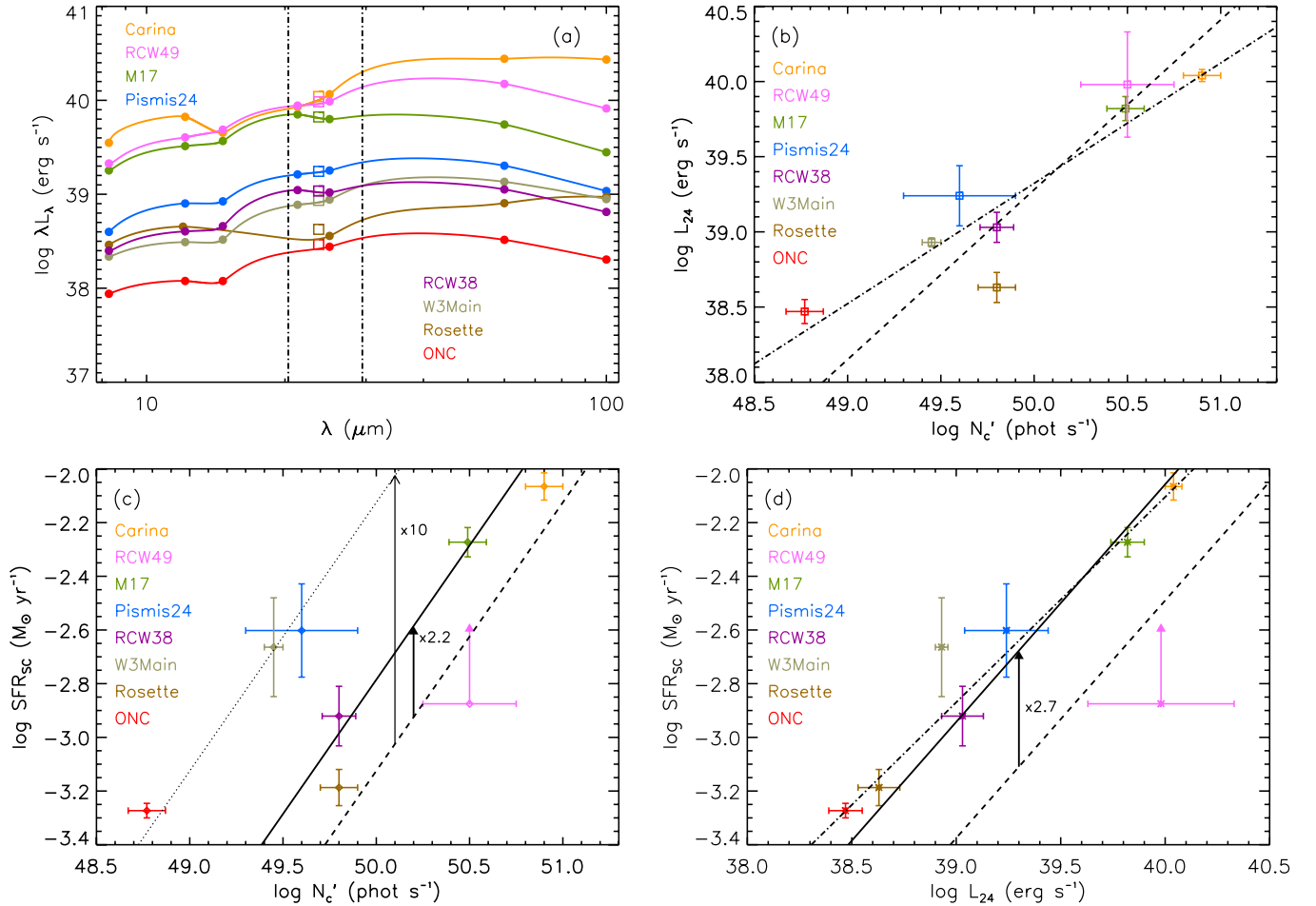
Figure 2. (a) Mid-IR SEDs (dots) for eight Galactic H II regions, from archival *IRAS* and *MSX* data. Solid curves are spline interpolations to the SEDs. Effective luminosities in the *Spitzer*/MIPS 24 μm bandpass (L_{24}; between the vertical dash-dotted lines) are plotted as boxes. (b) Plot of log L_{24} vs. log N_c', the uncorrected ionizing photon rate. The best fit to the data is plotted as a dash-dotted line with slope 0.80 ± 0.06. C+07 derived a super-linear relation (dashed line; slope 1.13 ± 0.03) for their extragalactic data. (c) SFRs derived from star counts, log $\mathrm{SFR_{SC}}$, plotted against log N_c'. The relation given in Equation (4), a standard extragalactic calibration, is marked as a dashed line. Versions of Equation (4) scaled up by factors of 2.2 (fitting the weighted mean of the data, excluding RCW 49 and the ONC) and 10 are plotted as solid and dotted lines, respectively. (d) Plot of log $\mathrm{SFR_{SC}}$ vs. L_{24}. The correlation between log $\mathrm{SFR_{SC}}$ and log L_{24} is consistent with the power-law relation derived by C+07 (dashed line) scaled up by a factor of 2.7 (solid line). The best-fit relation to our data is marked as a dash-dotted line and has a slope 0.76 ± 0.05.

(Section 4.1.2), expressed as

$$L_{\mathrm{P}\alpha} = 4\pi d^2 \frac{j(\mathrm{P}\alpha)}{j_\nu(ff)} F_\nu(\nu), \qquad (6)$$

where $j(\mathrm{P}\alpha)$ and $j_\nu(ff)$ are the Pα and free–free emissivities (Osterbrock 1974; Giles 1977) and $F_\nu(\nu)$ is the free–free radio continuum flux density at frequency ν (see Povich et al. 2007 for more detail). This gives $L_{\mathrm{P}\alpha} = 4.1 \times 10^{37}$ erg s^{-1}. Assuming again $d = 5$ Mpc and a 300 pc test aperture, log $S_{\mathrm{P}\alpha} = 38.76$, also within the range of values reported by C+07 (since it is based on radio observations, there is no need to correct the LSD for extinction).

Although M17 is a relatively low luminosity H II region in the extragalactic context, there is nothing unusual about its LSDs compared to the C+07 sample. An M17 analog would be observable in the *Spitzer* Infrared Nearby Galaxies Survey (SINGS; Kennicutt et al. 2003) 24 μm images as an H II knot in a nearby galaxy, assuming that it is not confused with a neighboring, brighter H II region, and it would fall well within the LSD distributions measured by C+07 for high-metallicity H II regions.

4.2. Comparison of Mid-IR Galactic and Extragalactic SFR Calibrations

We now generalize the analysis of M17 described above to a sample of eight Galactic H II regions (Table 2). With one exception, this sample consists of H II regions that, like M17, meet all of the following criteria: (1) ionized by at least one early O-type star (spectral type O5 V or earlier); (2) sufficiently embedded that the bulk of the bolometric luminosity is reprocessed by dust and emitted in the IR; (3) ionizing cluster(s) with well-sampled (complete to $m \lesssim 1.5\,M_\odot$) XLFs reported in the literature; and (4) evidence for ongoing star formation (for example, a detected population of stars with IR-excess emission from disks). The exception is the ONC, which lacks early O-type stars but was included because it serves as an observational touchstone for massive cluster studies in general, and XLF studies in particular. Table 2 contains data relevant to SFR determinations for each H II region.

Mass of stellar population. The total number of stars N_{pop} associated with the ionizing cluster(s) was adopted from published XLFs (see references listed in Table 2) and converted to total stellar mass, M_{pop}, for $m \geqslant 0.1\,M_\odot$ using the Kroupa IMF. Uncertainties on M_{pop} reflect only the statistical

Table 2
SFR Data for Eight Galactic H II Regions

Name	Alternate Name	d (kpc)	Earliest Known Star(s)	M_{pop} ($M_\odot$)	τ_{SF} (Myr)[a]	$\log L_{24}$ (erg s^{-1})[b]	$\log N_c'$ (photons s^{-1})[c]	SFR$_{SC}$ ($10^{-3} M_\odot$ yr^{-1})	Refs.[d]
Carina	NGC 3372	2.3 ± 0.1	LBV,WNL,O2 I	43000 ± 5000	5	40.04 ± 0.04	50.9 ± 0.1	8.6	1,2
RCW 49[e]	Wd 2	4.2 ± 1.5	$4\times$WNL,O3 V	>4000	3	39.98 ± 0.35	50.5 ± 0.3	>1.3	3,4
M17	NGC 6618	2.0 ± 0.1	$4\times$O4 V	8000 ± 1000	1.5	39.82 ± 0.08	50.5 ± 0.1	5.3	5,6,7
NGC 6357	Pismis 24	1.7 ± 0.5	O3.5 I, O3.5 III	6500 ± 1300	2	39.24 ± 0.20	49.6 ± 0.3	3.2	8,9,10
RCW 38		1.7 ± 0.2	O5.5 V	1200 ± 300	1	39.03 ± 0.10	49.8 ± 0.1	1.2	11
W3 Main		2.0 ± 0.07	Several $\sim$O5	3250 ± 1300	1.5	38.93 ± 0.03	49.45 ± 0.05	2.2	12
Rosette	NGC 2244	1.3 ± 0.1	O4 V	1300 ± 200	2	38.63 ± 0.10	49.8 ± 0.1	0.65	13,14
ONC	M42	0.41 ± 0.04	O7 V	1600 ± 100	3	38.48 ± 0.08	48.77 ± 0.09	0.53	15,16

Notes.

[a] The star formation timescale τ_{SF} is defined as the age of the *oldest* stars included in the IMF scaling that yielded M_{pop}. Hence, SFR$_{SC}$ is the time-averaged SFR over τ_{SF}, and the actual SFR during any short bursts could be significantly higher.

[b] $L_{24} \equiv \lambda L_\lambda$ is the equivalent mid-IR continuum luminosity in the MIPS 24 μm bandpass.

[c] N_c' is the Lyman continuum photon rate required to maintain the ionization of the radio H II region, following the notation and method of calculation employed by Smith et al. (1978).

[d] (1) Smith & Brooks 2007; (2) Povich et al. 2011; (3) Tsujimoto et al. 2007; (4) Ascenso et al. 2007; (5) Povich et al. 2007; (6) Broos et al. 2007; (7) Povich et al. 2009; (8) Wang et al. 2007; (9) Russeil et al. 2010; (10) Maíz Apellániz et al. 2007; (11) Wolk et al. 2006; (12) Feigelson & Townsley 2008; (13) Celnik 1985; (14) Wang et al. 2008; (15) Hillenbrand & Hartmann 1998; (16) Feigelson et al. 2002.

[e] M_{pop} and SFR$_{SC}$ are lower limits for RCW 49 because the 2.8 kpc distance (Ascenso et al. 2007) assumed for the IMF scaling is at the near end of the wide range of distance estimates reported in the literature.

uncertainties on N_{pop}, which include both the uncertain distance to each cluster and uncertainties introduced in extrapolating the XLFs to correct for incompleteness. Because we cannot always be certain that the XLF of a given cluster is complete, it may be safest to regard our reported M_{pop} values as lower limits.

Star formation timescale and SFR$_{SC}$. Following our selection criterion (4) above, we assume that star formation has been continuous over the lifetime of each H II region, defined as the star formation timescale τ_{SF}. While X-ray emission gives no useful constraint on the ages of the stars, follow-up optical and IR photometry of the X-ray detected stellar population does. Values of τ_{SF} for each region are based on published results from isochrone fitting to optical/near-IR color–magnitude diagrams (CMDs) and/or estimates of circumstellar disk fractions using observed IR excess emission. Age determinations for very young ($\sim$1 Myr) stellar populations in regions with ongoing star formation are notoriously imprecise, since the observed age spreads are generally comparable to the measurement uncertainties and the reported ages themselves. We therefore use the upper end of the range of ages reported in the recent literature (see references listed in Table 2) for each cluster. We had three motivations for this choice: (1) the difficulty in correcting for differential reddening in near-IR CMDs makes it easier to determine an upper age envelope than an average age for an obscured cluster. (2) Our values of M_{pop} may only be lower limits in some cases. (3) Our analysis of M17 (Section 4.1) indicates that, in spite of a $\sim$50% uncertainty on the age, SFR$_{SC}$ is significantly higher than SFR based on diffuse tracers; hence, we need only to place *lower* limits on the time-averaged SFR$_{SC} = M_{pop}/\tau_{SF}$ (Table 2) to test the generality of this result. We note that if there are bursts of higher SFR during the lifetime of an H II region, this would (temporarily) increase SFR$_{SC}$.

Mid-IR luminosity. Following Povich et al. (2007), we constructed IR SEDs for each H II region (Figure 2(a)), using aperture photometry to extract background-subtracted flux densities from archival *Infrared Astronomical Satellite* (*IRAS*; Neugebauer et al. 1984) and *Midcourse Space Experiment* (*MSX*; Price et al. 2001) survey images. We then performed a spline interpolation of the SED points, measured the equivalent

24 μm flux density $F_\nu(24)$ as the mean value of the interpolation within the MIPS 24 μm bandpass, and calculated L_{24} using Equation (5). The dominant source of uncertainty in L_{24} is the uncertain distance to each region (Table 2).

Ionizing photon rates from radio continuum emission. We calculated N_c' from the 5 GHz thermal radio continuum flux of each H II region using the same conversion as Smith et al. (1978). Because these regions are large on the sky, most of the integrated flux measurements come from single-dish observations that are decades old. Paladini et al. (2003) compiled data from several large surveys of Galactic radio H II regions, and we use these cataloged flux densities for all regions except the Carina Nebula and the Rosette, for which we adopt the values of Smith & Brooks (2007) and Celnik (1985), respectively. The available radio observations form a highly inhomogeneous data set, often suffering from background contamination and potentially unreliable calibration. We make no attempt to correct for internal absorption of ionizing photons and assume, as we found for the case of M17, that $N_c \approx N_c'$.

In Figure 2(b) we plot $\log L_{24}$ against $\log N_c'$, the relation that provides the foundation for the C+07 extragalactic mid-IR calibration, for which N_c is a direct proxy for SFR. We find a fairly tight correlation (rms scatter of 0.24 dex) with a marginally sub-linear slope ($\log L_{24} \propto [0.80 \pm 0.06] \log N_c'$; dash-dotted line). The most significant outlier is the Rosette, which is the only "extended low-surface brightness" radio H II region in the sample (Celnik 1985), and hence it is possible that its measured radio continuum flux density includes a significantly larger contribution from faint, extended emission compared to the other regions. C+07 derived a super-linear relation ($\log L_{24} \propto [1.13 \pm 0.03] \log N_c'$; dashed line) for their extragalactic relation and suggested that a linear relation could apply to low-luminosity H II regions. Our data would be consistent with a linear relation if the ONC were excluded from the sample.

In Figure 2(c) we compare SFR$_{SC}$ with N_c'. While H II regions with higher SFR$_{SC}$ also trend toward higher N_c', all points (except for RCW 49 for which SFR$_{SC}$ is a lower limit only) lie above the linear correlation expected from the extragalactic

calibration (Equation (4); plotted as a dashed line), some by as much as a factor of ∼10 (dotted line). The weighted mean offset of the data (excluding RCW 49 and the ONC) from the predicted correlation is a factor of 2.2 (solid line), with very large scatter (0.38 dex, rms). Note that the error bars on SFR_{SC} reflect only the uncertainty in M_{pop}, which is *not* independent of the uncertainty in N_c' (or L_{24} in Panel (d)) because both incorporate the distance uncertainty. The systematic offset from Equation (4) might be explained in part by correcting N_c' for absorption by dust and escape of ionizing photons, but this correction is unlikely to shift any points by more than a factor of ∼2, and as we showed for M17, some points would not shift at all.

In Figure 2(d), SFR_{SC} is plotted against L_{24}; this correlation is significantly tighter than the above comparisons of SFR_{SC} and N_c', with an rms scatter of 0.11 dex. The best-fit (dash-dotted; excludes RCW 49) line has a slope of 0.76±0.05, shallower than the 0.8850 slope of the analogous C+07 extragalactic relation (dashed line). The C+07 calibration, scaled up by a factor of 2.7 (solid line), best matches the weighted mean correlation between SFR_{SC} and L_{24}. Because our estimates of SFR_{SC} (Table 2) are lower limits, the factor of 2.7 represents a *minimum* systematic discrepancy between the mid-IR SFR calibrations and SFR measured from the resolved stellar populations.

There are several possible explanations for the decreased scatter in the SFR_{SC}–L_{24} correlation, compared with the SFR_{SC}–N_c' correlation, including region-to-region variations in the correction factor for N_c' to N_c, inhomogeneity of radio observations, and/or stochastic sampling of the high-mass tail of the IMF. The last possibility arises because ionizing photon rate produced by individual stars is a steeper function of mass than the bolometric luminosity, and hence in extreme cases only the single most massive star in a given region dominates N_c, while a wider range of stellar masses can heat dust and contribute to the 24 μm emission. If the mass of the most massive star is vulnerable to large, stochastic fluctuations from cluster to cluster, we might expect L_{24} to trace SFR more smoothly and with less scatter than N_c.

In summary, we find that SFR_{SC} derived from low- and intermediate-mass star counts to be systematically higher, by factors of at least two to three, compared to either the calibration of Equation (4) (Figure 2(c)) or the C+07 extragalactic SFR–L_{24} calibration (Figure 2(d)). The discrepancy between SFR_{SC} and SFR_{24} (or equivalently SFR_{ff}) we derived for the specific case of M17 (Section 4.1.3) therefore appears to be a general feature of Galactic H II regions. Parallels might be drawn between these results and the findings of Heiderman et al. (2010), who reported SFR surface densities measured from YSO counts in low-mass, Galactic molecular clouds that are higher by factors of 5–10 compared to the standard extragalactic Schmidt–Kennicutt Law (Kennicutt 1998b).

4.3. Systematics Affecting SFR Calibrations Based on Lyman Continuum Photon Rates

From the analysis in the preceding subsections, we conclude that even if Lyman continuum photon rates were known to arbitrarily high precision, an intrinsic, systematic uncertainty in the derived SFRs would remain. Specifically, it appears that the mid-IR SFR calibration of C+07 and, by extension, other calibrations that rely upon Lyman continuum photon rates underestimate SFRs by at least a factor of two to three (Figures 2(c) and (d)). This systematic affects the coefficient in Equation (4), the transformation between SFR and Lyman continuum photon production rate. The coefficient can be parameterized as $M_{pop}/(\tau N_c)$, where M_{pop}/N_c is the mass of a

young stellar population normalized by its production rate of Lyman continuum photons, and the timescale τ is either the duration of star formation traced by the observations of N_c or the lifetime of the ionizing stars, whichever is shorter. M_{pop}/N_c is itself a function of age in population synthesis models (e.g., the Starburst99 models; Vázquez & Leitherer 2005), but its functional form cannot be realistically modeled for cases where the SFR varies on timescales shorter than O-star lifetimes. As we cautioned in Section 2, Equation (4) strictly describes the SFR required to maintain a steady-state population of ionizing stars, implicitly assuming $\tau \approx 5$ Myr. Several effects likely to be important to M_{pop}/N_c and one important consequence of the assumed τ are discussed below.

4.3.1. Uncertain Lyman Continuum Photon Production Rates for O Stars

Fundamentally, $M_{pop}/N_c = (1/\eta) \sum_i (m/Q_0)_i$, where m/Q_0 is the ratio of stellar mass to Lyman continuum photon production for individual O stars and η is the (small) fraction of M_{pop} contained in O stars according to the assumed IMF. Values for Q_0 must be obtained from models of O stars as functions of spectral type and luminosity class. The Starburst99 grid of population synthesis models (Vázquez & Leitherer 2005) incorporates the modern O star calibrations and synthetic atmospheres of Smith et al. (2002) and Martins et al. (2005). These state-of-the-art calibrations employ non-LTE stellar dynamic atmosphere models that include the effects of line-blanketed winds and predict cooler effective temperatures by as much as ∼5000 K for the earliest spectral types. This results in ∼40% reductions of Q_0 for a given spectral type compared to earlier models (Panagia 1973; Vacca et al. 1996). Despite the obvious improvements in models of massive stars, we reiterate the caveat of Martins et al. (2005): the uncertainty on Q_0 remains a factor of ∼2 in any model; hence, its impact cannot be neglected, although it is unclear in which direction this uncertainty might bias SFR determinations.

4.3.2. The O Star Mass Discrepancy

The uncertainty in the numerator of m/Q_0 is also important. Model-based calibrations of O star parameters predict the stellar mass as a function of spectral type in two different ways. The emergent spectrum gives values for stellar luminosity L, effective temperature T_{eff}, and effective surface gravity g_{eff} measured from spectral line broadening, giving

$$M_{spec} = \frac{g_{eff} L}{4\pi G \sigma T_{eff}^4} \qquad (7)$$

(Vacca et al. 1996; Martins et al. 2005), where σ is the Stefan–Boltzmann constant and G is the gravitational constant. Alternatively, L and T_{eff} from stellar evolutionary tracks can be used to determine an evolutionary mass M_{evol}, which is associated with a stellar gravity g_{evol} (Vacca et al. 1996). In general, $g_{eff} < g_{evol}$, because a strong stellar wind lifts the surface layers of a star, reducing the gravity probed by spectral lines formed in the photosphere. Consequently, there is a discrepancy in the derived masses of up to a factor of ∼2, a systematic effect with $M_{spec} < M_{evol}$. O star masses based on M_{spec} in stellar models could therefore be underestimates, particularly for the earliest spectral types (Martins et al. 2005). This would tend to bias m/Q_0 downward in population synthesis models, leading to underestimates of M_{pop}/N_c and hence SFRs. Weidner & Vink (2010) recently found good agreement between

$M_{\rm spec}$ and dynamical masses calibrated to massive eclipsing binary systems, so it is possible that the O star mass discrepancy has been resolved.

4.3.3. The Upper Mass Limit of the IMF

The most massive stars ($m \geqslant 40\,M_\odot$) dominate N_c but represent only $\eta = 0.07$ of $M_{\rm pop}$ (assuming the Kroupa IMF) and follow, very approximately, the relation $Q_0(m) \propto m^{3.5}$. The ratio $M_{\rm pop}/N_c$ is therefore sensitive to the assumed upper mass limit of the IMF. This cutoff is poorly known; for example, Zinnecker & Yorke (2007) conclude that an upper limit of $150\,M_\odot$ is consistent with data, while Crowther et al. (2010) claim a maximum stellar mass of $300\,M_\odot$. This confusion may be compounded by mounting evidence that many O stars form in binary systems with nearly equal-mass components (Sana et al. 2008). Maíz Apellániz (2008) performed numerical experiments testing the effect on observational IMF determinations of mistaking unresolved massive binaries for single stars and concluded that while neglecting stellar multiplicity has a negligible effect on the high-mass IMF slope, the high-mass cutoff of the IMF will be systematically overestimated. In this work, we have conservatively assumed an upper mass limit of $100\,M_\odot$ (Equation (3)). Increasing this limit would decrease the SFR estimated from a given rate of ionizing photons, only worsening the discrepancy between $\rm SFR_{24}$ and $\rm SFR_{SC}$.

4.3.4. Runaway Massive Stars

Studies of massive stars in the field (remote from any significant episode of star formation) show that $\sim$10%–30% of O stars escape their natal star-forming regions (Gies 1987; Moffat et al. 1998; Oey & Lamb 2011). For young H II regions, O stars are likely ejected via dynamical encounters, which are enhanced by their high binary fraction (e.g., Leonard & Duncan 1990; Kroupa 2004); direct signatures of O-star escape can be seen in imaging of bow shocks (Gvaramadze et al. 2011). Although the loss of ionizing stars from H II regions could contribute to the discrepancy between $\rm SFR_{24}$ and $\rm SFR_{SC}$, it cannot account for the full magnitude of the discrepancy.

4.3.5. The Assumed Form of the IMF

Fundamentally, the discrepancy between $\rm SFR_{SC}$ and $\rm SFR_{24}$ may indicate that $M_{\rm pop}/N_c$ predicted by stellar population synthesis models is systematically too low or, equivalently, the fraction of mass η contained in massive stars is too high. A straightforward way to increase $M_{\rm pop}/N_c$ would be to increase the numbers of low-mass stars (which contain the bulk of the stellar mass) relative to massive stars (which dominate the luminosity in young populations). This is equivalent to steepening the intermediate-mass (or super-solar) IMF slope. In their recent review, Bastian et al. (2010) argue that there is no convincing evidence for strong IMF variations, but this conclusion does not amount to a claim that the form of the "universal" IMF is known to high precision. As is the case with SFRs, IMF *comparisons* across different environments are more reliable than *absolute* measurements. Indeed, Figure 2 of Bastian et al. (2010) reveals that while derivations of Γ in the super-solar mass regime are broadly consistent with the Salpeter–Kroupa slope ($\Gamma = 1.3$), this actually represents only a lower bound on Γ reported for $1.5\,M_\odot < m < 5\,M_\odot$. At intermediate masses, the IMF slopes cluster around $\Gamma' = 1.7$ (Scalo 1998).

If we alter our standard Kroupa IMF (Equations (1)–(3)) by increasing $\Gamma = 1.3$ to $\Gamma' = 1.7$ for $1.5\,M_\odot < m <$

$5\,M_\odot$, we derive $\rm SFR'_{24} = \eta/\eta' \times \rm SFR_{24} = 1.4 \times \rm SFR_{24}$. We also find $\rm SFR'_{SC} = 0.9 \times \rm SFR_{SC}$ by normalizing both IMFs to the same $N_{\rm pop}$. A steeper intermediate-mass IMF slope marginally reduces SFRs based on low/intermediate-mass star counts while significantly increasing SFRs derived from massive star diagnostics, driving the independent measurements toward convergence. The combined effect produces a factor of $\sim$1.6($= 1.4/0.9$) increase in $\rm SFR_{24}/\rm SFR_{SC}$, enough to explain much of the systematic discrepancy.

It would be reasonable to question the appropriateness of altering the IMF used in the XLF scaling method, given that a fundamental assumption of this method is similarity with the ONC IMF (Section 4.1.1). Hence, we note that the benchmark ONC IMF of Muench et al. (2002) was measured using low-mass stars only ($m < 2\,M_\odot$; see Figure 1) and $\Gamma = 1.21$ was simply extrapolated to the high-mass tail. In spite of its status as the nearest "massive" young cluster, the ONC contains too few intermediate-mass stars to support a statistical measurement of the super-solar IMF slope. We conclude that a super-solar IMF slope steeper than Salpeter is not excluded by existing IMF determinations, and our method for comparing SFRs derived from XLF scaling and massive star tracers can indirectly constrain its value.

4.3.6. Stochastic Sampling of the IMF

In the limit of very low SFR, the linear calibration of SFR against ionizing photon rate (Equation (4)) must break down, as star formation can occur without producing any massive stars in a given region. In the case of most Galactic H II regions, we must consider the intermediate possibility that the high-mass tail of the IMF will not be fully sampled. To representatively sample the high-mass tail of the IMF, a stellar population should contain $\gtrsim 10$ O stars (Cerviño & Valls-Gabaud 2003), which corresponds to $M_{\rm pop} = 2900\,M_\odot$ (assuming a Kroupa or Chabrier IMF; Lee et al. 2009). Cerviño et al. (2003) also find that a total stellar mass of $\sim$3000$\,M_\odot$ is the lowest mass for which sampling effects can be ignored (for a young stellar population and solar metallicity). Similarly, da Silva et al. (2011) find that, after accounting for stochastic effects, Lyman continuum fluxes are consistent on average with those expected for a fully sampled IMF for SFRs $\gtrsim 10^{-3}\,M_\odot\,{\rm yr}^{-1}$ (although the scatter in $N_c/\rm SFR$ is significant for $\rm SFR = 10^{-3}\,M_\odot\,{\rm yr}^{-1}$, approximately a factor of two). For $\rm SFR = 10^{-4}\,M_\odot\,{\rm yr}^{-1}$, the average ionizing luminosity is suppressed by a factor of $\sim$2.

The eight Galactic H II regions described in Table 2 span a wide range of $M_{\rm pop}$ and SFRs, with some significantly above these limits (Carina, M17) and others well below them (ONC, Rosette). In the lowest-mass regions, we might therefore expect calibrations based on population synthesis models with fully sampled IMFs to underestimate SFR. However, stochastic sampling cannot explain the systematic offset of *all* H II regions in our sample, including the high-mass regions Carina and M17 that fully sample the IMF, from the C+07 relation. We note that the best-fit line to the $\rm SFR_{SC}$–L_{24} relation (Figure 2(d)) has a shallower slope than the C+07 correlation, as would be expected if L_{24} preferentially underestimates SFRs in the lower-mass regions, such as the ONC.

4.3.7. Star Formation Timescales

As shown in Table 2, the (upper limit) ages for our Galactic H II region sample range from 1 to 5 Myr, with a median age of 2 Myr. These young ages are a consequence of our selection criterion (2) that most of the bolometric luminosity

be reprocessed by warm dust and reradiated in the mid-IR. Older Galactic H II regions have been excluded from our analysis because they do *not* exhibit bright mid-IR nebulosity and would not be identifiable as 24 μm point sources in a SINGS image of an external galaxy; hence they would not have been included in the C+07 calibration sample. Prominent excluded clusters include Westerlund 1, one of the most massive young clusters in the Milky Way (Clark et al. 2005), and several Red Supergiant Clusters (Figer et al. 2006; Davies et al. 2007; Alexander et al. 2009), all of which contain significant populations of Wolf–Rayet stars, yellow hypergiants, red supergiants, and other evolved massive stars. The ages of these clusters fall in the 5–20 Myr range, and hence they represent the future evolution of the giant H II regions in our sample. The dust in such evolved H II regions has either been destroyed by the hard radiation field or blown away by stellar winds and possibly supernovae, removing the source of the bright mid-IR emission. Such regions certainly contribute to the extended IR emission of the Galaxy, since very little of their bolometric luminosity is reprocessed locally by dust. The integrated Galactic IR emission is dominated by cool dust with a significant component coming from older stars (e.g., Misiriotis et al. 2006), whereas the SEDs of young Galactic H II regions are dominated by warm dust heated by O stars (Figure 2(a)).

The median value for the timescale τ_{SF} used to calculate SFR_{SC} is a factor of ~2.5 times lower than O-star lifetimes, the timescale assumed implicitly by the C+07 calibration and other calibrations based on population synthesis models, like Equation (4) (see the caveat in Section 2). Hence the discrepancy between SFR_{SC} and L_{24} (or N'_c) in very young regions could be resolved by applying this correction factor to the calibrations of SFR versus diffuse emission tracers.

The C+07 H II region sample was selected on the basis of compact, bright "knots" of mid-IR emission. Based on the discussion above, this selection criterion likely imposed an age constraint of $\tau_{SF} \lesssim 5$ Myr, which means that *absolute* SFRs derived by C+07 and similar studies of individual extragalactic star-forming regions could be systematically underestimated by factors of $\gtrsim 8$ Myr/5 Myr $= 1.6$, where 8 Myr is the steady-state timescale assumed implicitly by population synthesis (Section 2) and 5 Myr is the *maximum* age of a mid-IR bright H II region. We note that the H II region models employed by C+07 neglected H II region expansion, stellar winds, and supernovae, without which H II regions could remain mid-IR bright throughout the lifetime of the ionizing stars. This discrepancy due to assumed timescales should not affect studies like K+09, where SFRs are measured as averages over entire galaxies (although care is needed in the case of dwarf galaxies and other systems subject to short bursts of star formation). In the case of normal spiral galaxies like the Milky Way, it is usually a good approximation that the galaxy-wide SFR has been constant over the last ~100 Myr, and the calibration of Equation (4) should hold. Indeed, K+09 find that IR traces SFR more weakly in their data than in the C+07 sample, consistent with the longer timescales traced by galaxy-wide Hα and IR emission.

5. ARE GLOBAL GALACTIC SFR ESTIMATES CONSISTENT WITH EXTRAGALACTIC DIAGNOSTICS?

As we have seen, SFR estimates depend on a wide range of assumptions; incorrect input assumptions can lead to potentially large systematic errors in absolute SFR determinations. In addition, we must keep in mind that different assumptions may be appropriate in different observational regimes, complicating attempts to compare SFRs. For example, if one set of assumptions were valid in external galaxies (which are often measured as wholes) while a different set of assumptions held in the Milky Way (where star formation is often studied piecemeal, and always in projection), these inputs could lead to a discrepancy between SFRs in the Milky Way and other galaxies.

As reviewed in Section 3, significant effort has been invested in measuring the Galactic SFR, but if we were external observers located Mpc from the Galaxy, would we still measure a Milky Way SFR of ~2 $M_\odot$ yr^{-1}? The answer to this question is critical for comparing the Milky Way with other galaxies and extrapolating the detailed knowledge we gain in our Galaxy to more distant systems. Here we present two tests that can assess, directly and with a minimum of assumptions, whether the Galactic SFR is consistent with extragalactic SFR calibrations. Although preliminary, these tests can serve as valuable sanity checks for our comparison of the Galactic SFR with calibrations used in other galaxies.

5.1. The Brightest Radio Supernova Remnant (Cassiopeia A)

The LFs of radio SNRs have been observed in ~20 galaxies and can be modeled as power laws with constant index and scaling that depends roughly linearly on SFR (Chomiuk & Wilcots 2009, hereafter CW09). Unfortunately, it is very difficult to establish a complete sample of SNRs in the Milky Way (e.g., Green 2005), so a comparison of the full LF is not a plausible technique for estimating the Galactic SFR. However, CW09 showed that there is a good correlation between a galaxy's SFR and the radio spectral luminosity of its most radio-bright SNR (L_{max}). We can use this L_{max}–SFR correlation to make an independent estimate of the Galactic SFR, assuming that Cas A is the most luminous SNR in the Milky Way. This is a valid assumption because any SNR with a similar luminosity to Cas A would be bright enough for inclusion in any modern catalog, even if it were located on the far side of the Galaxy (Green 2004). The details of our extragalactic sample are described in the Appendix; SFRs are measured using the K+09 calibration of Hα and total IR emission. Here we measure SNR luminosities at 4.85 GHz because this frequency is less susceptible to the free–free absorption that can dampen lower-frequency radio continuum emission in starburst galaxies.

There is a clear correlation between L_{max} and SFR (Figure 3), best fit at 4.85 GHz as

$$L_{max}^{4.85} = \left(85^{+22}_{-17}\right) SFR^{1.11 \pm 0.15}. \qquad (8)$$

This fit is shown as a solid line in Figure 3. This correlation is consistent with stochastic sampling of the power-law SNR LF (measured as described in the Appendix and CW09), marked as a dashed line in Figure 3. The scatter in the L_{max}–SFR correlation is ± 0.51 dex, consistent with the scatter expected from stochastic sampling of a power law (± 0.55 dex).

We note that IC 10 is a clear outlier (marked as a filled circle in Figure 3); its large "superbubble" ($\gtrsim 130$ pc; Yang & Skillman 1993) is much more luminous than expected for a galaxy with IC 10's SFR. Yang & Skillman (1993) claim that the most likely explanation for this source is multiple SNRs overlapping in the vicinity of a giant H II region. In fact, many of the brightest SNRs in galaxies may not be typical of the SNR population as a whole, and they are likely to be a rather heterogeneous class of objects (Chu et al. 1999). Some may be the combined emission from several overlapping SNRs (Yang & Skillman 1993) or
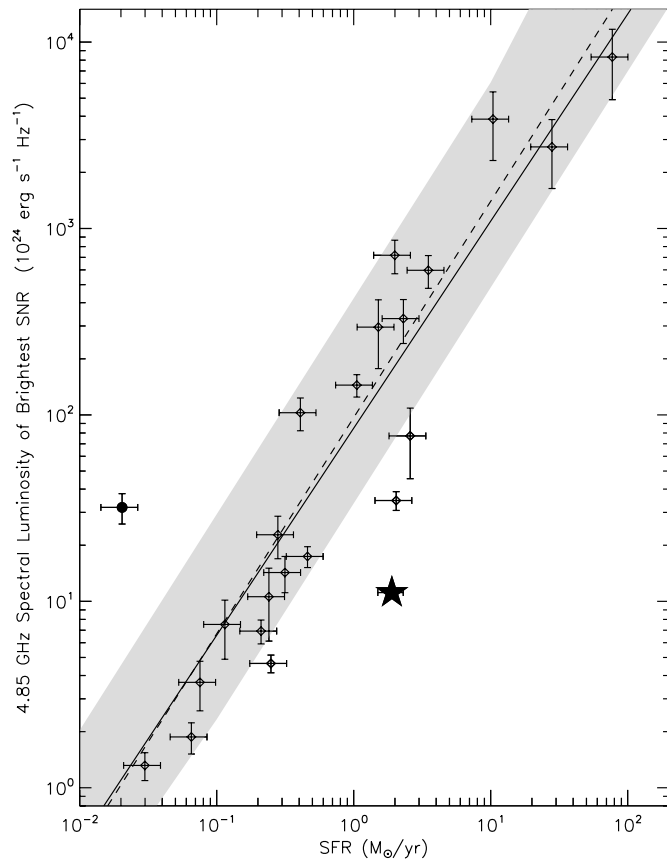
Figure 3. For each galaxy in our sample, we plot the 4.85 GHz radio luminosity of its brightest SNR as a function of the galaxy's SFR. The solid line marks the best fit to the data. The dashed line represents the expected correlation due to random statistical sampling of a power-law LF, and the gray shaded region shows the expected 1σ variation in the correlation due to stochasticity. The point marked by a filled circle is the outlier IC 10. The Milky Way is represented by a black star, assuming that the Milky Way's most luminous SNR is Cas A and its SFR is $1.9 \pm 0.4 \, M_\odot \, \mathrm{yr}^{-1}$.

the remnants of hypernovae/gamma-ray bursts (Lozinskaya & Moiseev 2007). Others may be interacting with unusually dense circumstellar material blown off by the progenitor star (e.g., the luminous SNR in NGC 4449; Milisavljevic & Fesen 2008). Others may not be SNRs at all—Pakull & Grisé (2008) point out that many large-diameter (200–500 pc) bright radio bubbles are likely blown by the jets of ultraluminous X-ray sources (ULXs) and not by SNe. For example, in the most luminous radio "SNR" in NGC 7793 (S26; Pannuti et al. 2002), Pakull & Grisé (2008) uncover a jet-like structure via high-resolution X-ray imaging which spans the ~450 pc radio bubble and implies that that this bubble is blown by a microquasar and not by SN activity. Regardless of the physical mechanisms driving the L_{max}–SFR relation, it appears to hold empirically across more than three orders of magnitude, and we can use it as a test of current estimates of the Galactic SFR.

In Figure 3, we plot the luminosity of Cas A and a Galactic SFR of $1.9 \pm 0.4 \, M_\odot \, \mathrm{yr}^{-1}$ (as found in Section 3), marked with a solid star. The Milky Way appears to deviate from the L_{max}–SFR relation as the most outlying point besides IC 10. Using the technique described in the Appendix, we calculate a 0.2% probability that, given the luminosity of Cas A, the SFR of the Milky Way is $1.9 \pm 0.4 \, M_\odot \, \mathrm{yr}^{-1}$ (or, a 3% probability that it is $>1 \, M_\odot \, \mathrm{yr}^{-1}$). Given the inherent uncertainty in the L_{max}–SFR relation and the fact that outliers like IC 10 do exist,

we cannot conclusively eliminate the possibility that Galactic SFR estimates and extragalactic SFR diagnostics are consistent with one another. However, it is worth noting that the observed offset of the Milky Way from the L_{max}–SFR relation implies that either the Galactic SFR has been overestimated or that extragalactic SFRs have been systematically underestimated.
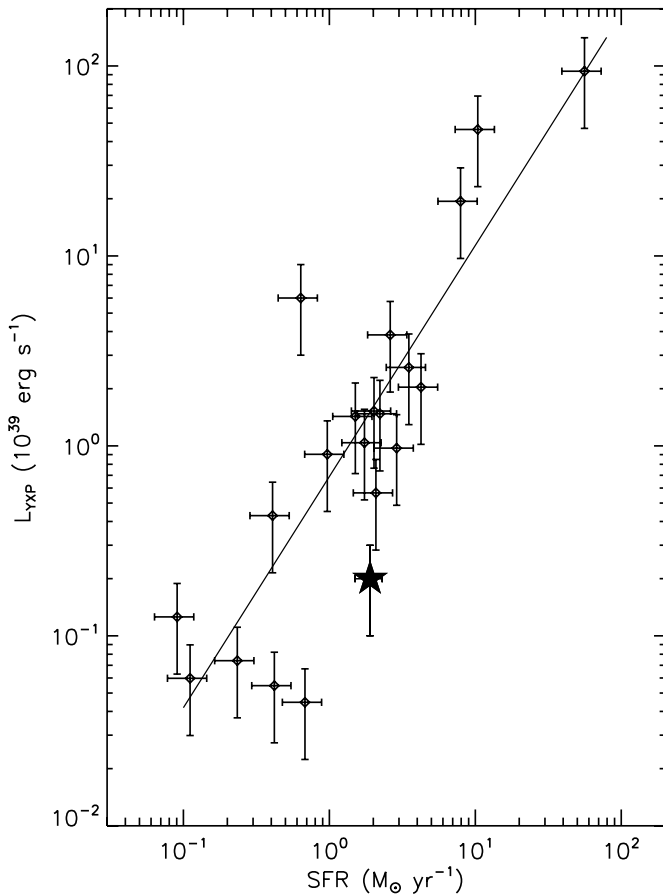
5.2. Luminous Young X-Ray Point Sources

We can further test whether the measured Galactic SFR is consistent with SFR determinations in other galaxies using young X-ray point sources (YXPs). The X-ray emission from galaxies has often been claimed to trace SFR (e.g., Grimm et al. 2003; Ranalli et al. 2003; Mineo et al. 2011) because of the high luminosities from high-mass X-ray binaries (HMXBs), in addition to SNRs and ULXs.

Grimm et al. (2002) studied what the Milky Way X-ray source population would look like to an outside observer and estimated a total luminosity of $L_{\mathrm{HMXB}} = (2 \pm 1) \times 10^{38} \, \mathrm{erg} \, \mathrm{s}^{-1}$ over 2–10 keV for HMXBs. We also add the luminosity of the Crab Nebula ($L_{\mathrm{X}} = 1 \times 10^{38} \, \mathrm{erg} \, \mathrm{s}^{-1}$ assuming a distance of 2 kpc; Grimm et al. 2002; Davidson & Fesen 1985), which dominates the Milky Way's SNR luminosity in the X-ray band. The Milky Way does not host any ULXs, so its $L_{\mathrm{YXP}} = (3 \pm 1) \times 10^{38} \, \mathrm{erg} \, \mathrm{s}^{-1}$.

We can compare the Milky Way with the sample of 20 "local normal and starburst" galaxies in Persic & Rephaeli (2007), for which there are X-ray point-source LFs in the literature. Persic & Rephaeli acknowledge that the major uncertainty in using the X-ray point-source luminosity as an SFR indicator is contamination by low-mass X-ray binaries (LMXBs), which are associated with older stellar populations and trace stellar mass rather than SFR. In the case of the Milky Way, the integrated luminosity of LMXBs is ten times greater than that of HMXBs (Grimm et al. 2002). Fortunately, the relative number of HMXBs compared with LMXBs should be a function of SFR divided by a galaxy's stellar mass (Gilfanov et al. 2004). Persic & Rephaeli (2007) deal with LMXB contamination by assuming that X-ray point-source LFs in systems with high SFR are representative of the young component and universally applicable; similarly, they assume that LFs measured in E/S0 galaxies represent the old population of X-ray point sources. They fit each galaxy's LF with a combination of old and young components. In Figure 4, we plot the product of their measured point-source luminosities and YXP fractions, rescaled to the distances listed in Kennicutt et al. (2008) and Moustakas & Kennicutt (2006). We calculate SFRs as described in the Appendix, using the K+09 calibration.

In Figure 4, we see that there is indeed a correlation between L_{YXP} and SFR. The Milky Way, assuming an SFR of $1.9 \pm 0.4 \, M_\odot \, \mathrm{yr}^{-1}$, is marked as a star. The standard deviation around the best-fit line is 0.47 dex, and the Milky Way is located ~1.5σ from the correlation. The Milky Way's deviation corresponds to an unusually high SFR for its measured L_{YXP}, an offset in the same direction as observed for the L_{max}–SFR relation. Recently, Mineo et al. (2011) pointed out that the Persic & Rephaeli correlation is offset downward from other X-ray binary–SFR relations in the literature by a factor of ~2–2.5, fitting unusually low L_{YXP} values as a function of SFR. They hypothesize that Persic & Rephaeli (2007) have overestimated the contribution from the old population of X-ray sources; if this is true, it would imply that the discrepancy of the Milky Way from the L_{YXP}–SFR relation is larger than that shown in Figure 4. In addition, Lehmer et al. (2010) show that the Milky Way is a slight (~1σ) outlier from their X-ray calibration to external galaxies. They find that

Figure 4. Integrated 2–10 keV luminosity of young X-ray point sources in each of 20 nearby galaxies (Persic & Rephaeli 2007) plotted against SFR (assuming 50% uncertainty on L_{YXP}). The best-fit correlation is marked as a solid black line. The Milky Way is plotted as a black star, assuming the SFR from Section 3 of $1.9 \pm 0.4 \, M_\odot \, yr^{-1}$ and HMXB luminosity from Grimm et al. (2002).

given the Milky Way's mass ($5 \times 10^{10} \, M_\odot$; Hammer et al. 2007) and SFR (assumed to be $2.0 \, M_\odot \, yr^{-1}$, in good agreement with that used here), the ratio of X-ray luminosity in LMXBs compared with HMXBs should be ~ 1.4, almost an order of magnitude lower than the $L_{LMXB}/L_{HMXB} \approx 10$ measured for the Milky Way by Grimm et al. (2002). This is consistent with an SFR of $2.0 \, M_\odot \, yr^{-1}$ for the Milky Way being higher than expected from extragalactic calibrations.

5.3. Is the Milky Way an Outlier?

The Milky Way appears to deviate from both the L_{YXP}–SFR and L_{max}–SFR relations at the 1σ–3σ level, consistently showing a higher SFR than expected from the extragalactic relations. This deviation is marginal, and the Milky Way's similar offset from both correlations might simply be a coincidence, so we cannot eliminate the possibility that the Milky Way's measured SFR is consistent with extragalactic determinations. However, both the SNR and YXP tests hint that a Galactic SFR of $2 \, M_\odot \, yr^{-1}$ may be higher than we would measure for the Milky Way if we were external observers using the K+09 SFR calibration. If this is true, there are three possible explanations for the difference: (1) estimates of SFR are biased high in the Milky Way (compared with "absolute" SFRs), (2) estimates of SFR are biased low in external galaxies, and/or (3) the Milky Way is a fundamentally outlying system (as suggested by Hammer et al. 2007).

If this deviation is real, it is unlikely to be related to the differences between Galactic H II regions and extragalactic calibrations described in Section 4.2. Assuming that the most luminous SNR and the YXP population roughly trace the counts of massive stars, and understanding that the SFRs used in the L_{YXP}–SFR and L_{max}–SFR relations are predominately measurements of the Lyman continuum rate, the Milky Way's displacement from the L_{max}/L_{YXP}–SFR relations implies that available measurements of N'_c and L_{24} *overestimate* the Galactic SFR, whereas we have found that these quantities *underestimate* SFRs in individual Galactic H II regions. If the offsets described in Section 4.2 are due to a poorly constrained (but universal) IMF shape, they will affect the Milky Way and external galaxies equally, while differences due to assumptions about star formation timescales should be irrelevant when we average over entire galaxies (including the Milky Way).

It is therefore difficult to explain the potential offset of the Milky Way from the L_{max}/L_{YXP}–SFR relations, but we must keep in mind that the Galactic SFR remains quite uncertain. For example, to calculate a total ionizing luminosity for the Milky Way from their catalog of *WMAP* H II regions, Murray & Rahman (2010) had to make at least three significant assumptions, each of which increases the Galactic SFR by $\sim 40\%$–100% with large uncertainty: (1) they multiply their measured N'_c by two to correct for distant H II regions missing from their catalog; (2) they multiply by 1.5 to account for the diffuse component of the *WMAP* free–free emission, assuming this diffuse component has the same distribution as the detected H II regions; and (3) they multiply by 1.37 to correct for Lyman continuum escape and absorption by dust (detail given in McKee & Williams 1997; note that the K+09 extragalactic calibration should also account for dust absorption, because it uses a combination of Hα and IR emission). In addition, if one-third of the free–free emission has a very diffuse, smooth distribution as Murray & Rahman (2010) assert, some of this low-surface brightness emission may go undetected in external galaxies, leading to an underestimate of extragalactic SFRs. Additional strategies for comparison between the Milky Way and external galaxies, along with better statistics on the L_{max}/L_{YXP}–SFR correlation, are required to test the provocative implication that the Galactic SFR may be overestimated, and/or extragalactic SFRs may be underestimated, by a factor of a few.

6. CONCLUSIONS

After normalizing published estimates of the Galactic SFR to Starburst99 population synthesis models and a Kroupa IMF, measurements converge to a Galactic SFR of $1.9 \pm 0.4 \, M_\odot \, yr^{-1}$.

We test to see if SFR estimates in the Milky Way are consistent with extragalactic SFR diagnostics, using luminous SNRs and YXPs; the results are noisy, but the Milky Way is a 1σ–3σ outlier in both tests, implying that perhaps the SFR of the Milky Way is overestimated and/or extragalactic SFRs are systematically underestimated.

We also test for consistency between SFR diagnostics within Galactic H II regions, where we can obtain exquisite detail and actual star counts. Our comparison of SFRs based on tracers of massive stars against SFRs determined from star counts reveals that large systematic errors persist in *absolute* SFR determinations. In particular, measurements of SFRs in both the Milky Way and external galaxies could be underestimating absolute SFRs by factors of at least two to three. Two outstanding issues may explain the discrepancy between SFR_{SC} and SFRs measured from indirect tracers.

1. *Uncertainty in the form of the intermediate-mass IMF*. The systematic offset would be assuaged if the IMF has a slope that is steeper than Salpeter across the super-solar mass range ($1.5\ M_\odot < m < 5\ M_\odot$), a tweak that is fully consistent with current data (Bastian et al. 2010).

2. *Systematically overestimated star formation timescales for extragalactic H II regions*. The population synthesis models employed in extragalactic SFR determinations often assume that the duration of star formation is longer than an O star lifetime. This assumption breaks down in the case of H II regions that are mid-IR bright, because such regions are systematically younger than the O-star lifetimes by factors of $\gtrsim 1.6$.

We stress that these systematic issues are not mutually exclusive, and we cannot rule out additional contributions from the O star models themselves (Smith et al. 2002; Martins et al. 2005) and runaway O stars. In addition, SFR determinations in the lowest-mass H II regions ($<3000\ M_\odot$) will also be affected by stochastic undersampling of the high-mass end of the IMF. Because we derived only lower limits on SFR_{SC}, the actual discrepancy may be higher than reported here.

Nevertheless, distinguishing between the two primary scenarios is crucial to our understanding of absolute SFRs. In the IMF scenario, *all* Galactic and extragalactic SFR determinations must be revised upward, with far-reaching implications for applications that rely on absolute SFRs, like the Schmidt–Kennicutt relation, galaxy evolution models, and chemical enrichment by evolved low-mass stars. For example, if SFRs were larger on galaxy-wide scales, this would increase the discrepancy between SFR integrated over cosmic time and measured stellar mass densities (Wilkins et al. 2008; Choi & Nagamine 2011). Also (assuming the Galactic SFR has been roughly constant throughout the history of the Milky Way), a larger amount of fresh unprocessed ISM material would be required to infall onto the Galactic disk to explain stellar abundance patterns and sustain star formation (e.g., Sancisi et al. 2008).

On the other hand, if the timescale scenario is sufficient to explain the discrepancy between SFR_{SC} and the calibrations based on population synthesis models in a sample of IR-bright, H II regions, only SFR determinations in localized, very young star-forming regions will be affected, not entire galaxies. The extragalactic Hα+IR SFR calibration of K+09, for example, accounts for the ionizing luminosity of all massive stars in a galaxy, averaging across the star formation histories of many H II regions, so it should not be vulnerable to this systematic effect.

Our discussion reminds us that implicit assumptions have the potential to significantly impact SFR determinations, both in a relative and absolute sense. In the future, additional tests and larger sample sizes are required to test the significance of the potential deviation of the Milky Way's SFR from extragalactic calibrations. Meanwhile, additional multiwavelength observations of Galactic star-forming regions with a range of ages will have the power to discern between the two most likely scenarios for the H II-region SFR discrepancy. Such observations would allow for a more accurate determination of the IMF and also provide additional estimates of SFR_{SC} for a range of star formation histories. This should pave the way to an independent, empirical calibration of absolute SFR versus tracers of ionizing luminosity. In order to place studies of galaxy evolution, ISM physics, and stellar populations on the most solid footing possible, we need to continue toward a better understanding

of the systematics affecting SFR determinations, ensuring that Galactic and extragalactic calibrations achieve convergence.

APPENDIX

DETAILS OF THE L_{max}–SFR RELATION

In an attempt to include as many galaxies as possible on the L_{max}–SFR relation described in Section 5.1, we compile SNRs at 4.85 GHz, as opposed to the 1.45 GHz data used in CW09. Free–free and synchrotron-self absorption can greatly reduce the lower frequency ($\sim$1–2 GHz) radio continuum signal coming from SNRs in very dense, violently star-forming systems. However, frequencies around $\sim$5 GHz remain unabsorbed (e.g., Parra et al. 2007) and are therefore ideal for searching for SNRs in starbursts. 4.85 GHz SNR samples are selected by the criteria described in CW09 and from the same references, with the addition of a few galaxies: NGC 1808 (radio data from Saikia et al. 1990 and Collison et al. 1994; excluding 58.56 − 36.3, which is probably the AGN nucleus of the galaxy; Jiménez-Bailón et al. 2005); NGC 4038/4039 (Neff & Ulvestad 2000); and Arp 299 (Pérez-Torres et al. 2009 and Ulvestad 2009). In contrast with CW09, here we include the superbubble in IC 10. Although it is a severe outlier, being unusually luminous for a galaxy with IC 10's SFR, we cannot exclude it on these grounds alone as it might have an important impact on the L_{max}–SFR relation.

To calculate the luminosity of Cas A, we use a 4.85 GHz flux density of 806 Jy (Baars et al. 1977). The luminosity of Cas A is fading with time (by $\sim$1% per year; Baars et al. 1977), and these flux densities are standardized to epoch 1980.0. We use a distance of 3.4 kpc to Cas A (Reed et al. 1995). The fact that the luminosity of Cas A is decreasing implies that the Milky Way's position on the L_{max}–SFR relation will change with time, but we note that this is also likely true for the other galaxies on the relation. This fact underscores the point that the L_{max}–SFR relation is a statistical and stochastic relation; for it to hold true, as the most luminous SNR fades, another must be born and rise to take its place.

Shortly after the analysis of CW09 was published, a new calibration for Hα+IR SFRs was released by K+09. Unlike the previous C+07 SFR calibration, the K+09 formulation is calibrated to entire galaxies, not individual star-forming regions. To calculate the extragalactic SFRs, we use the Hα+total IR (TIR) calibration from K+09, described as

$$\text{SFR}\ (M_\odot\ \text{yr}^{-1}) = 5.5 \times 10^{-42}\ (L_{H\alpha} + 0.0024\ L_{TIR}), \quad \text{(A1)}$$

where $L_{H\alpha}$ and L_{TIR} are both in units of erg s^{-1}, $L_{H\alpha}$ is corrected for foreground Galactic extinction, and L_{TIR} is a linear combination of luminosity measurements in the *IRAS* 25, 60, and 100 μm bands as suggested by Dale & Helou (2002). Distances and Hα measurements come from Kennicutt et al. (2008) if

Table 3
Galaxies Used in the L_{max}–SFR Relation for SNRs

Galaxy	R.A. (2000)[a] (hr:min:sec)	Decl. (2000)[a] (°:′:″)	Type[a]	Distance (Mpc)	SFR ($M_\odot$ yr^{-1})	SFR Frac	FoV (arcmin)	N_{SNR} (4.85 GHz)
LMC	05:23:34.5	−69:45:22	SB(s)m	0.05 ± 0.003	0.21	1.0	600	26
SMC	00:52:44.8	−72:49:43	SB(s)m pec	0.06 ± 0.003	0.03	1.0	270	11
IC 10	00:20:17.3	+59:18:14	IBm[b]	0.66 ± 0.03	0.02	0.91	4.3	4
M 33	01:33:50.9	+30:39:36	SA(s)cd	0.84 ± 0.04	0.25	0.98	40	35
NGC 1569	04:30:49.0	+64:50:53	IBm	1.9 ± 0.4	0.24	1.0	2.2	18
NGC 300	00:54:53.5	−37:41:04	SA(s)d	2.00 ± 0.10	0.10	0.65	9	8
NGC 4214	12:15:39.2	+36:19:37	IAB(s)m	2.92 ± 0.29	0.15	0.77	2.2	3
NGC 2366	07:28:54.6	+69:12:57	IB(s)m	3.19 ± 0.32	0.08	1.0	4.6	4
M 82	09:55:52.7	+69:40:46	I0	3.53 ± 0.35	3.51	1.0	0.5	23
M 81	09:55:33.2	+69:03:55	SA(s)ab	3.63 ± 0.18	0.52	0.88	12.5	3
NGC 7793	23:57:49.8	−32:35:28	SA(s)d	3.91 ± 0.39	0.28	1.0	9	4
NGC 253	00:47:33.1	−25:17:18	SAB(s)c	3.94 ± 0.39	2.89	0.69	2.75	18
NGC 4449	12:28:11.9	+44:05:40	IBm	4.21 ± 0.42	0.41	1.0	5	5
M 83	13:37:00.9	−29:51:56	SAB(s)c	4.47 ± 0.22	2.08	0.98	9	14
NGC 4736	12:50:53.0	+41:07:14	(R)SA(r)ab	4.66 ± 0.47	0.39	0.81	2	10
NGC 6946	20:34:52.3	+60:09:14	SAB(rs)cd	5.9 ± 1.2	2.61	0.99	9	21
NGC 4258	12:18:57.5	+47:18:14	SAB(s)bc	7.98 ± 0.40	1.33	0.79	7	4
M 51	13:29:55.7	+47:13:53	SAbc	8.00 ± 1.04	2.30	1.0	9	30
NGC 1808	05:07:42.3	−37:30:47	(R)SAB(s)b	10.6 ± 2.1	2.52	0.60	0.3	10
NGC 4038/39	12:01:53.3	−18:52:37	Pec	25.0 ± 5.0	10.4	1.0	2	35
Arp 299	11:28:32.2	+58:33:44	Pec	50.6 ± 10.1	56.0	0.5	0.01	19
Arp 220	15:34:57.1	+23:30:11	Pec	85.2 ± 17.0	77.2	1.0	0.02	12

Notes.
[a] From NED.
[b] From de Vaucouleurs & Freeman (1972).

available, and if not, from Moustakas & Kennicutt (2006). *IRAS* measurements come predominantly from Sanders et al. (2003), but also from Fullmer & Lonsdale (1989), Moshir et al. (1992), Hunter et al. (1986), and Rice et al. (1988). Basic information on the sample galaxies and derived SFRs can be found in Table 3.

Table 3 also lists the number of SNRs (N_{SNR}) in the complete samples at 4.85 GHz. Many SNR surveys do not cover the entire extent of the galaxy, so we also include the field of view (FoV) of the SNR survey, and the fraction of the SFR covered in this FoV (SFR Frac). The SFRs used in the L_{max}–SFR relation are the measured SFRs times these fractions.

As in CW09, we find that the SNR LF can be described as a power law: $n(L) = A\,L^\beta$. Using the techniques described in CW09, we find, for the 4.85 GHz data, a best-fit power-law index of $\beta = -2.02$ and near-linear scaling of the LF with SFR as

$$A_{4.85} = \left(75^{+19}_{-15}\right) \text{SFR}^{1.19\pm0.11}. \qquad (A2)$$

These measurements of the SNR LF allow us to quantify the fact that galaxies with higher SFRs are more likely to host very luminous SNRs because they have larger populations of SNRs.

We can quantify the probability that the Galactic SFR converged upon in Section 3 is consistent with the L_{max}–SFR relation by assuming that (1) the L_{max}–SFR relation is the result of stochastic sampling of a power law and (2) the power-law scaling can be described by Equation (A2). For a given SFR, we then calculate how many SNRs can be expected for a power law with this scaling, and Monte Carlo sample that number of SNRs from the power-law distribution 10^4 times. This then provides 10^4 values of L_{max} for the given SFR, and we repeat this process for a range of SFRs from 0.005 to 20 $M_\odot$ yr^{-1}. For each SFR, we measure what fraction of these L_{max} values fall within a factor of 1.5 of the luminosity of Cas A. This probability as a function of SFR has a roughly lognormal form, peaking at 0.2 $M_\odot$ yr^{-1}.

If we use the 1.4 GHz data presented in CW09 (which has a smaller sample size than the 4.85 GHz data) for an analysis of the Milky Way on the L_{max}–SFR relation, we find that the Milky Way is offset from the correlation in the same direction, although it is less aberrant (giving a 15% chance that the SFR of the Milky Way is $1.9 \pm 0.4\ M_\odot$ yr^{-1}).

REFERENCES

Alexander, M. J., Kobulnicky, H. A., Clemens, D. P., et al. 2009, AJ, 137, 4824
Ascenso, J., Alves, J., Beletsky, Y., & Lago, M. T. V. T. 2007, A&A, 466, 137
Baars, J. W. M., Genzel, R., Pauliny-Toth, I. I. K., & Witzel, A. 1977, A&A, 61, 99
Bastian, N., Covey, K. R., & Meyer, M. R. 2010, ARA&A, 48, 339
Bennett, C. L., Fixsen, D. J., Hinshaw, G., et al. 1994, ApJ, 434, 587
Bertelli, G., Bressan, A., Chiosi, C., Fagotto, F., & Nasi, E. 1994, A&AS, 106, 275
Bouwens, R. J., Illingworth, G. D., Oesch, P. A., et al. 2011, ApJ, 737, 90
Broos, P. S., Feigelson, E. D., Townsley, L. K., et al. 2007, ApJS, 169, 353
Calzetti, D., Kennicutt, R. C., Engelbracht, C. W., et al. 2007, ApJ, 666, 870 (C+07)
Calzetti, D., Sheth, K., Churchwell, E., & Jackson, J. 2009, in Proc. 4th Spitzer Center Conf.: The Evolving ISM in the Milky Way and Nearby Galaxies, ed. K. Sheth, A. Noriega-Crespo, J. Ingalls, & R. Paladini, http://ssc.spitzer.caltech.edu/mtgs/ismevol/
Carey, S. J., Noriega-Crespo, A., Mizuno, D. R., et al. 2009, PASP, 121, 76
Celnik, W. E. 1985, A&A, 144, 171
Cerviño, M., Luridiana, V., Pérez, E., Vílchez, J. M., & Valls-Gabaud, D. 2003, A&A, 407, 177
Cerviño, M., & Valls-Gabaud, D. 2003, MNRAS, 338, 481
Chabrier, G. 2003, PASP, 115, 763
Chabrier, G. 2005, in The Initial Mass Function 50 Years Later, ed. E. Corbelli, F. Palla, & H. Zinnecker (Astrophysics and Space Science Library, Vol. 327; Dordrecht: Springer), 41
Chiappini, C., Matteucci, F., & Gratton, R. 1997, ApJ, 477, 765
Choi, J.-H., & Nagamine, K. 2011, arXiv:1101.5656
Chomiuk, L., & Wilcots, E. M. 2009, ApJ, 703, 370 (CW09)

Chu, Y., Chen, C., & Lai, S. 1999, in HST May Symposium, The Largest Explosions Since the Big Bang: Supernovae and Gamma Ray Bursts, ed. M. Livio, N. Panagia, & K. Sahu (Cambridge: Cambridge Univ.), 131

Churchwell, E., Babler, B. L., Meade, M. R., et al. 2009, PASP, 121, 213

Clark, J. S., Negueruela, I., Crowther, P. A., & Goodwin, S. P. 2005, A&A, 434, 949

Collison, P. M., Saikia, D. J., Pedlar, A., Axon, D. J., & Unger, S. W. 1994, MNRAS, 268, 203

Cox, P., Kruegel, E., & Mezger, P. G. 1986, A&A, 155, 380

Crowther, P. A., Schnurr, O., Hirschi, R., et al. 2010, MNRAS, 408, 731

Dale, D. A., & Helou, G. 2002, ApJ, 576, 159

da Silva, R. L., Fumagalli, M., & Krumholz, M. 2011, arXiv:1106.3072

Davidson, K., & Fesen, R. A. 1985, ARA&A, 23, 119

Davies, B., Figer, D. F., Kudritzki, R.-P., et al. 2007, ApJ, 671, 781

Davies, B., Hoare, M. G., Lumsden, S. L., et al. 2011, MNRAS, 416, 972

de Rossi, M. E., Tissera, P. B., De Lucia, G., & Kauffmann, G. 2009, MNRAS, 395, 210

de Vaucouleurs, G., & Freeman, K. C. 1972, Vistas Astron., 14, 163

Diehl, R., Halloin, H., Kretschmer, K., et al. 2006, Nature, 439, 45

Feigelson, E. D., Broos, P., Gaffney, J. A., III, et al. 2002, ApJ, 574, 258

Feigelson, E. D., Getman, K. V., Townsley, L. K., et al. 2011, ApJS, 194, 9

Feigelson, E. D., & Townsley, L. K. 2008, ApJ, 673, 354

Figer, D. F., MacKenty, J. W., Robberto, M., et al. 2006, ApJ, 643, 1166

Fioc, M., & Rocca-Volmerange, B. 1997, A&A, 326, 950

Fullmer, L., & Lonsdale, C. J. 1989, JPL D-1932, Version 2, part no. 3 (Pasadena, CA: Jet Propulsion Lab.)

Gagné, M., Fehon, G., Savoy, M. R., et al. 2011, ApJS, 194, 5

Getman, K. V., Feigelson, E. D., Grosso, N., et al. 2005, ApJS, 160, 353

Getman, K. V., Feigelson, E. D., Townsley, L., et al. 2006, ApJS, 163, 306

Gies, D. R. 1987, ApJS, 64, 545

Giles, K. 1977, MNRAS, 180, 57P

Gilfanov, M., Grimm, H., & Sunyaev, R. 2004, MNRAS, 347, L57

Green, D. A. 2004, Bull. Astron. Soc. India, 32, 335

Green, D. A. 2005, Mem. Soc. Astron. Ital., 76, 534

Grimm, H., Gilfanov, M., & Sunyaev, R. 2002, A&A, 391, 923

Grimm, H.-J., Gilfanov, M., & Sunyaev, R. 2003, MNRAS, 339, 793

Güsten, R., & Mezger, P. G. 1982, Vistas Astron., 26, 159

Gvaramadze, V. V., Kniazev, A. Y., Kroupa, P., & Oh, S. 2011, A&A, in press (arXiv:1109.2116)

Hammer, F., Puech, M., Chemin, L., Flores, H., & Lehnert, M. D. 2007, ApJ, 662, 322

Hanson, M. M., & Popescu, B. 2008, in IAU Symp. 250, Massive Stars as Cosmic Engines, ed. F. Bresolin, P. A. Crowther, & J. Puls (Cambridge: Cambridge Univ. Press), 307

Heiderman, A., Evans, N. J., II, Allen, L. E., Huard, T., & Heyer, M. 2010, ApJ, 723, 1019

Hillenbrand, L. A., & Hartmann, L. W. 1998, ApJ, 492, 540

Hunter, D. A., Gillett, F. C., Gallagher, J. S., III, Rice, W. L., & Low, F. J. 1986, ApJ, 303, 171

Jiménez-Bailón, E., Santos-Lleó, M., Dahlem, M., et al. 2005, A&A, 442, 861

Kauffmann, G., & Haehnelt, M. 2000, MNRAS, 311, 576

Kennicutt, R. C., Hao, C-N., Calzetti, D., et al. 2009, ApJ, 703, 1672 (K+09)

Kennicutt, R. C., Jr. 1998a, ARA&A, 36, 189

Kennicutt, R. C., Jr. 1998b, ApJ, 498, 541

Kennicutt, R. C., Jr., Armus, L., Bendo, G., et al. 2003, PASP, 115, 928

Kennicutt, R. C., Jr., Lee, J. C., Funes, J. G., et al. 2008, ApJS, 178, 247

Kennicutt, R. C., Jr., Tamblyn, P., & Congdon, C. E. 1994, ApJ, 435, 22

Koenig, X. P., & Allen, L. E. 2011, ApJ, 726, 18

Kroupa, P. 2001, MNRAS, 322, 231

Kroupa, P. 2004, New Astron. Rev., 48, 47

Kroupa, P., & Weidner, C. 2003, ApJ, 598, 1076

Larson, R. B. 1974, MNRAS, 169, 229

Lee, J. C., Gil de Paz, A., Tremonti, C., et al. 2009, ApJ, 706, 599

Lehmer, B. D., Alexander, D. M., Bauer, F. E., et al. 2010, ApJ, 724, 559

Leitherer, C., Schaerer, D., Goldader, J. D., et al. 1999, ApJS, 123, 3

Leonard, P. J. T., & Duncan, M. J. 1990, AJ, 99, 608

Limongi, M., & Chieffi, A. 2006, ApJ, 647, 483

Lozinskaya, T. A., & Moiseev, A. V. 2007, MNRAS, 381, L26

Madau, P., Ferguson, H. C., Dickinson, M. E., et al. 1996, MNRAS, 283, 1388

Maíz Apellániz, J. 2008, ApJ, 677, 1278

Maíz Apellániz, J., Walborn, N. R., Morrell, N. I., Niemela, V. S., & Nelan, E. P. 2007, ApJ, 660, 1480

Martins, F., Schaerer, D., & Hillier, D. J. 2005, A&A, 436, 1049

McKee, C. F., & Williams, J. P. 1997, ApJ, 476, 144

Mezger, P. G. 1987, in Starbursts and Galaxy Evolution, ed. T. X. Thuan, T. Montmerle, & J. Tran Thanh Van (Paris: Editions Frontieres), 3

Mezger, P. G., Smith, L. F., & Churchwell, E. 1974, A&A, 32, 269

Milisavljevic, D., & Fesen, R. A. 2008, ApJ, 677, 306

Miller, G. E., & Scalo, J. M. 1979, ApJS, 41, 513

Mineo, S., Gilfanov, M., & Sunyaev, R. 2011, arXiv:1105.4610

Misiriotis, A., Papadakis, I. E., Kylafis, N. D., & Papamastorakis, J. 2004, A&A, 417, 39

Misiriotis, A., Xilouris, E. M., Papamastorakis, J., Boumis, P., & Goudis, C. D. 2006, A&A, 459, 113

Moffat, A. F. J., Marchenko, S. V., Seggewiss, W., et al. 1998, A&A, 331, 949

Moshir, M., Kopman, G., & Conrow, T. A. O. 1992, IRAS Faint Source Survey, Explanatory Supplement Version 2 (Pasadena, CA: Infrared Processing and Analysis Center, California Institute of Technology)

Moustakas, J., & Kennicutt, R. C., Jr. 2006, ApJS, 164, 81

Muench, A. A., Lada, E. A., Lada, C. J., & Alves, J. 2002, ApJ, 573, 366

Murray, N., & Rahman, M. 2010, ApJ, 709, 424

Neff, S. G., & Ulvestad, J. S. 2000, AJ, 120, 670

Neugebauer, G., Habing, H. J., van Duinen, R., et al. 1984, ApJ, 278, L1

Oey, M. S., & Lamb, J. B. 2011, arXiv:1109.0759

Osterbrock, D. E. 1974, Astrophysics of Gaseous Nebulae (San Francisco, CA: Freeman)

Pakull, M. W., & Grisé, F. 2008, in AIP Conf. Ser. 1010, A Population Explosion: The Nature and Evolution of X-ray Binaries in Diverse Environments, ed. R. M. Bandyopadhyay, S. Wachter, D. Gelino, & C. R. Gelino (Melville, NY: AIP), 303

Paladini, R., Burigana, C., Davies, R. D., et al. 2003, A&A, 397, 213

Panagia, N. 1973, AJ, 78, 929

Pannuti, T. G., Duric, N., Lacey, C. K., et al. 2002, ApJ, 565, 966

Parra, R., Conway, J. E., Diamond, P. J., et al. 2007, ApJ, 659, 314

Pérez-Torres, M. A., Romero-Cañizales, C., Alberdi, A., & Polatidis, A. 2009, A&A, 507, L17

Persic, M., & Rephaeli, Y. 2007, A&A, 463, 481

Povich, M. S., Benjamin, R. A., Whitney, B. A., et al. 2008, ApJ, 689, 242

Povich, M. S., Churchwell, E., Bieging, J. H., et al. 2009, ApJ, 696, 1278

Povich, M. S., Smith, N., Majewski, S. R., et al. 2011, ApJS, 194, 14

Povich, M. S., Stone, J. M., Churchwell, E., et al. 2007, ApJ, 660, 346

Povich, M. S., & Whitney, B. A. 2010, ApJ, 714, L285

Preibisch, T., & Feigelson, E. D. 2005, ApJS, 160, 390

Price, S. D., Egan, M. P., Carey, S. J., Mizuno, D. R., & Kuchar, T. A. 2001, AJ, 121, 2819

Ranalli, P., Comastri, A., & Setti, G. 2003, A&A, 399, 39

Reed, B. C. 2005, AJ, 130, 1652

Reed, J. E., Hester, J. J., Fabian, A. C., & Winkler, P. F. 1995, ApJ, 440, 706

Rice, W., Lonsdale, C. J., Soifer, B. T., et al. 1988, ApJS, 68, 91

Robitaille, T. P., Meade, M. R., Babler, B. L., et al. 2008, AJ, 136, 2413

Robitaille, T. P., & Whitney, B. A. 2010, ApJ, 710, L11

Russeil, D., Zavagno, A., Motte, F., et al. 2010, A&A, 515, A55

Saikia, D. J., Unger, S. W., Pedlar, A., et al. 1990, MNRAS, 245, 397

Salpeter, E. E. 1955, ApJ, 121, 161

Sana, H., Gosset, E., Nazé, Y., Rauw, G., & Linder, N. 2008, MNRAS, 386, 447

Sancisi, R., Fraternali, F., Oosterloo, T., & van der Hulst, T. 2008, A&AR, 15, 189

Sanders, D. B., Mazzarella, J. M., Kim, D.-C., Surace, J. A., & Soifer, B. T. 2003, AJ, 126, 1607

Scalo, J. 1998, in ASP Conf. Ser. 142, The Stellar Initial Mass Function (38th Herstmonceux Conference), ed. G. Gilmore & D. Howell (San Francisco, CA: ASP), 201

Siess, L., Dufour, E., & Forestini, M. 2000, A&A, 358, 593

Smith, L. F., Biermann, P., & Mezger, P. G. 1978, A&A, 66, 65

Smith, L. J., Norris, R. P. F., & Crowther, P. A. 2002, MNRAS, 337, 1309

Smith, N., & Brooks, K. J. 2007, MNRAS, 379, 1279

Tsujimoto, M., Feigelson, E. D., Townsley, L. K., et al. 2007, ApJ, 665, 719

Ulvestad, J. S. 2009, AJ, 138, 1529

Vacca, W. D., Garmany, C. D., & Shull, J. M. 1996, ApJ, 460, 914

Vázquez, G. A., & Leitherer, C. 2005, ApJ, 621, 695

Wang, J., Townsley, L. K., Feigelson, E. D., et al. 2007, ApJS, 168, 100

Wang, J., Townsley, L. K., Feigelson, E. D., et al. 2008, ApJ, 675, 464

Weidner, C., & Vink, J. S. 2010, A&A, 524, A98

Wilkins, S. M., Trentham, N., & Hopkins, A. M. 2008, MNRAS, 385, 687

Wolk, S. J., Spitzbart, B. D., Bourke, T. L., & Alves, J. 2006, AJ, 132, 1100

Xu, Y., Moscadelli, L., Reid, M. J., et al. 2011, ApJ, 733, 25

Yang, H., & Skillman, E. D. 1993, AJ, 106, 1448

Zinnecker, H., & Yorke, H. W. 2007, ARA&A, 45, 481